

Finite-amplitude Rayleigh–Bénard convection and pattern selection for viscoelastic fluids

By ZHENYU LI AND ROGER E. KHAYAT†

Department of Mechanical & Materials Engineering, The University of Western Ontario,
London, Ontario, Canada N6A 5B9
rkhayat@eng.uwo.ca

(Received 10 October 2003 and in revised form 22 November 2004)

The influence of inertia and elasticity on the onset and stability of Rayleigh–Bénard thermal convection is examined for highly elastic polymeric solutions with constant viscosity. These solutions are known as Boger fluids, and their rheology is approximated by the Oldroyd-B constitutive equation. The Galerkin projection method is used to obtain the departure from the conduction state. The solution is capable of displaying complex dynamical behaviour for viscoelastic fluids in the elastic and inertio-elastic ranges, which correspond to $Ra < Ra_c^s$ and $Ra > Ra_c^s$, respectively, Ra_c^s being the critical Rayleigh number at which stationary thermal convection emerges. This behaviour is reminiscent of that observed experimentally for viscoelastic Taylor–Couette flow. For a given Ra in the pre-critical range, finite-amplitude periodic oscillatory convection emerges when the elasticity number, E , exceeds a threshold. Periodicity is lost as E increases, leading to a T^2 quasi-periodic behaviour, and the breakup of the torus as E increases further. Although no experimental data are available for direct comparison, this scenario is reminiscent of the flow sequence observed by Muller *et al.* (1993) in the Taylor–Couette flow of a Boger fluid. Stationary thermal convection emerges, via a supercritical bifurcation, when Ra exceeds Ra_c^s . The amplitude of motion is found to be little influenced by fluid elasticity or retardation time, especially as the Rayleigh number increases. However, the range of stability of the stationary thermal convection narrows considerably for viscoelastic fluids. In this case, oscillatory thermal convection is favoured. The onset and the stability of other steady convective patterns, namely hexagons and squares, are studied in the inertio-elastic range by using an amplitude equation approach. The range of stability of each pattern is examined, simultaneously allowing the validation of the two-dimensional picture.

1. Introduction

While the problem of Rayleigh–Bénard (RB) convection has been extensively investigated for Newtonian fluids, relatively little attention has been devoted to the thermal convection of viscoelastic fluids. Flow instability and turbulence are far less widespread in viscoelastic fluids than in Newtonian fluids because of the high viscosity of polymeric fluids. Green (1968), Vest & Arpaci (1969), and Sokolov & Tanner (1972) were the first to conduct a linear stability analysis of a layer of an upper-convected Maxwell fluid, in which stress exhibits an elastic response to strain characterized by a single viscous relaxation time, λ . The relaxation time is scaled by the thermal

† Author to whom correspondence should be addressed.

diffusion time D^2/κ (D is the height of the fluid layer and κ is the thermal diffusivity) to yield the dimensionless elasticity number, $E = \lambda\kappa/D^2$, which is taken as a measure of elasticity or normal stress effects that lead to the Weissenberg rod-climbing and other viscoelastic phenomena (Boger & Walters 1993). Nonlinear RB convection of non-Newtonian fluids was considered by Eltayeb (1977), Rosenblat (1986), Martínez-Mardones & Pérez-García (1992), Harder (1991), and, more recently by Khayat (1994, 1995*a, b*, 1996), Park & Lee (1996), Martínez-Mardones *et al.* (1996), and Parmentier, Lebon & Regnier (2000).

Linear stability analysis suggests that, for a sufficiently large elasticity number and a sufficiently large Prandtl number $Pr = \nu/\kappa$ (ν being the kinematic viscosity), there is a competition between the processes of viscous relaxation and thermal diffusion that causes the first convective instability to be oscillatory (overstability) rather than stationary. For fixed Prandtl number, the critical Rayleigh number for the onset of oscillatory convection decreases as a function of increasing E . Kolodner (1998) reports that for $Pr = 10$, which is typical of room-temperature liquids such as water, the oscillatory threshold is less than the threshold for the onset of stationary RB convection for all $E > 0.05$. Thus, sufficiently viscoelastic fluids (with only moderately small elasticity number) should exhibit oscillatory convection. In general, viscoelastic instability is observed in polymer melts as well as in polymer solutions, which usually consist of a Newtonian solvent and a polymeric solute. These solutions are often highly elastic but have an essentially constant viscosity. They are known as Boger fluids and are reasonably well represented by the Oldroyd-B constitutive model (Bird, Armstrong & Hassager 1987).

Khayat investigated nonlinear RB convection of viscoelastic (1994, 1995*a, b*) and shear-thinning (1996) fluids by adopting a four-dimensional dynamical system. Such a system constitutes a generalization of the Lorenz model (Lorenz 1963) to include elastic normal stress effects. It was found that for very weakly elastic fluids, stationary convection loses its stability to oscillatory convection via a Hopf bifurcation when the Rayleigh number exceeds a critical value Ra_c^h in the post-critical range ($Ra_c^h > Ra_c^s$). Unlike Ra_c^s , Ra_c^h depends strongly on fluid elasticity and viscosity ratio. In contrast to Newtonian fluids, in elastic fluids, stationary convection is lost to periodic rather than directly to irregular motion, but eventually the periodicity is lost as the Rayleigh number is further increased. It was also found that elasticity tends to precipitate the loss of periodicity, while the viscosity ratio tends to delay it. Martínez-Mardones & Pérez-García (1992) studied the linear convective stability of the Jeffreys model as well. An overstability was predicted when the retardation-to-relaxation-time ratio is smaller than a critical value that depends on E and Pr . Both free-free and the more realistic rigid-rigid boundary conditions were considered in their analysis. Changing the nature of the boundary conditions produced only quantitative differences in the results. The free-free boundary conditions were also adopted by Brand & Zielinska (1986) who examined the onset of convection of a Maxwell fluid. Their investigation is based on amplitude equations similar to the Ginzburg-Landau equation for Newtonian fluids (Drazin & Reid 1981). They proved the existence of a tri-critical co-dimension-2 (CT) point at which the conduction, stationary convection, and oscillatory convection states meet. Phase diagrams near the CT bifurcation points were also analysed by Zielinska, Mukamel & Steinburg (1986). At the CT points the oscillatory and stationary modes become unstable simultaneously. Parmentier *et al.* (2000) examined the Bénard-Marangoni instability for various viscoelastic models, including the lower convective, the upper convective and the co-rotational Jefferys models. In particular, they investigated the range of parameter conditions for the onset of stability of

stationary rolls, squares and hexagonal cells. However, little if any attention was paid to the onset of oscillatory convection, which is the most dangerous mode for viscoelastic fluids.

Despite the theoretical interest in oscillatory viscoelastic convection, this overstability has been difficult to observe in reality until recently (Tanner 1983; Larson 1992; Kolodner 1998). Some of the earlier experiments were conducted by Liang & Acrivos (1970). Their study, however, focused on the effects of shear thinning, which were found to enhance regularity in flow pattern. More recently, Kolodner (1998) examined the convection of buffer solutions of long DNA strands in an annular geometry. Convective patterns were found to take the form of spatially localized standing and travelling waves that exhibit small amplitude and extremely long oscillation periods. The critical Rayleigh number for the onset of overstability is lower than for a Newtonian fluid, which is in agreement with linear stability analysis of viscoelastic fluids.

The objective of the present paper is to investigate the onset and stability of finite-amplitude RB convection with relatively dominant elastic effects. The fluid is assumed to be a polymeric solution obeying the Oldroyd-B equation. Given the complexity of the viscoelastic problem, two-dimensional flow is covered first in some detail. A dynamical systems approach is adopted for the solution. Although both experiment (Kolodner 1998) and theory (Parmentier *et al.* 2000) indicate that two-dimensional rolls are favoured at the onset of oscillatory or stationary convection, the emergence of three-dimensional patterns can be important, and will be investigated. The prevalence of two-dimensional rolls, similarly to Newtonian flow, should be expected only at the onset of convection, where the velocity gradients and therefore normal stresses remain relatively weak.

2. Problem formulation and solution procedure

Consider an incompressible viscoelastic fluid of relaxation time λ , viscosity η , specific heat at constant pressure C_p , and thermal conductivity K . In this study, only fluids that can be reasonably represented by a single relaxation time and constant viscosity are considered. The fluid is confined between two infinite and flat plates at $Z = -D/2$ and $Z = D/2$. Typically, the fluid examined is a polymeric solution composed of a Newtonian solvent and a polymeric solute of viscosities η_s and η_p , respectively. Thus, $\eta = \eta_s + \eta_p$. A polyacrylamide solution in a maltose syrup/water mixture typically constitutes such a fluid (Walters 1980). Note that the retardation time of the fluid is equal to $\lambda\eta_s/\eta$ (Bird *et al.* 1987).

2.1. General equations and boundary conditions

Let T_0 and $T_0 + \delta T$ be the temperatures of the upper and lower plates, respectively, with δT being the temperature difference. T_0 is taken as the reference temperature. In the present work, the substances of main interest are assumed to obey the following equation of state:

$$\rho(T) = \rho_0[1 - \alpha_T(T - T_0)], \quad (1)$$

where ρ and ρ_0 are the densities at the temperatures T and T_0 , respectively, and α_T is the coefficient of volumetric expansion. Let D , D^2/κ , κ/D , $\rho_0\kappa^2/D^2$, be, respectively, typical length, time, velocity and pressure, and $\eta\kappa/D^2$ be the typical stress. Here $\kappa = K/(\rho_0 C_p)$ is the thermal diffusivity. If the Boussinesq approximation, which states that the effect of compressibility is negligible everywhere in the conservation equations except in the buoyancy term, is assumed to hold, then the non-dimensional equations

for the conservation of mass, momentum and energy, are, respectively

$$\nabla \cdot \mathbf{u} = 0, \quad (2)$$

$$Pr^{-1}(\mathbf{u}_{,t} + \mathbf{u} \cdot \nabla \mathbf{u}) = -\nabla p + \theta \mathbf{e}_z + \frac{Rv}{Rv + 1} \Delta \mathbf{u} + \nabla \cdot \boldsymbol{\tau}, \quad (3)$$

$$\theta_{,t} + \mathbf{u} \cdot \nabla \theta = \Delta \theta + Ra \mathbf{u} \cdot \mathbf{e}_z \quad (4)$$

where ∇ is the gradient operator, and Δ is the Laplacian operator. A subscript after a comma denotes partial differentiation; t is the time, \mathbf{u} is the velocity vector, p is the pressure deviation from the steady state, and \mathbf{e}_z is the unit vector in the direction opposite to gravity. $\theta = g\alpha_T D^3(T - T_s)/(\nu\kappa)$ is the departure from the steady-state temperature, $T_s = T_0 - (z - 1/2)\delta T$, where g is the acceleration due to gravity, and $\nu = \eta/\rho_0$ is the kinematic viscosity. In this work, the rheology of the fluid is approximated by the Oldroyd-B constitutive model (Bird *et al.* 1987) so that the elastic part of the deviatoric stress tensor, $\boldsymbol{\tau}$, is governed by the following equation:

$$E [\boldsymbol{\tau}_{,t} + \mathbf{u} \cdot \nabla \boldsymbol{\tau} - (\nabla \mathbf{u})^T \cdot \boldsymbol{\tau} - \boldsymbol{\tau} \cdot \nabla \mathbf{u}] = -\boldsymbol{\tau} + \frac{1}{Rv + 1} \dot{\boldsymbol{\gamma}}, \quad (5)$$

where T denotes matrix transposition, and $\dot{\boldsymbol{\gamma}} = \nabla \mathbf{u} + (\nabla \mathbf{u})^T$ is the rate-of-strain tensor.

The Oldroyd-B constitutive model is rather elementary as it does not account for the rate-of-strain dependence of transport coefficients (viscosity and relaxation time), nor does it include the spectrum of relaxation times usually characteristic of polymeric fluids. However, this constitutive model is adopted in this study for four main reasons. First, since the aim of the study is to examine the influence of elasticity on the stability of thermal convection, the Oldroyd-B model does represent adequately highly elastic (Boger) fluids, for which the viscosity remains sensibly constant over a wide range of shear rates. A polyacrylamide solution in a maltose syrup/water mixture typically constitutes such a fluid (Walters 1980). Second, the Oldroyd-B constitutive equation is one of the simplest viscoelastic laws that accounts for normal stress effects (which lead to the Weissenberg rod-climbing phenomenon), which are responsible for the periodic phenomena arising in viscoelastic fluids. Other more realistic phenomenological or molecular-theory-based models (Bird *et al.* 1987; Tanner 1983) will probably lead to a different stability picture (Larson 1988). For instance, the presence of shear thinning, which is not accounted for by the Oldroyd-B equation, can be destabilizing since the *effective* Rayleigh number increases as the viscosity decreases with increasing shear rate (Khayat 1996; Larson 1988). Third, the present formulation is a nonlinear stability analysis, which emphasizes the interplay between inertia and normal stress effects during the transition from the conduction state to steady or oscillatory thermal convection. Nonlinear behaviour is adequately reflected in the convective terms in the momentum equation and the upper-convective terms in the Oldroyd-B equation. Fourth, and most importantly, almost all experimental measurements and flow visualization so far reported on the instability of viscoelastic flows have been conducted on Boger fluids. Comparison between theory and experiment becomes possible when the Oldroyd-B constitutive equation is used. However, the inclusion of a distribution of relaxation times allows the constitutive model to cover a wider range of practical fluids. Another simple nonlinear constitutive model that has been studied in the literature is the lower-convective Oldroyd-A model. Identical results were obtained for these two models in linear stability analysis (Eltayeb 1977; Martinez-Mardones & Perez-Garcia 1990). No substantial difference has been observed in weakly nonlinear stability analysis (Martinez-Mardones *et al.* 1996; Parmentier *et al.* 2000). Larson (1988) also

showed that the secondary normal stress difference, N_2 , of the Oldroyd-A model is equal in magnitude to the primary normal stress difference, N_1 , and is of opposite sign. Thus, the ratio $N_2/N_1 = -1$ is much too large, however, since experiments usually suggest N_2/N_1 is on the order of $-1/10$. For this reason, and because the Oldroyd-A model has no molecular basis, while the Oldroyd-B model does, the Oldroyd-A model will not be considered here.

There are four important dimensionless groups in the problem, namely the Rayleigh number, Ra , the Prandtl number, Pr , the elasticity number, E , and the solvent-to-solute viscosity ratio, Rv :

$$Ra = \frac{\delta T g \alpha_T D^3}{\nu \kappa}, \quad Pr = \frac{\nu}{\kappa}, \quad E = \frac{\lambda \kappa}{D^2}, \quad Rv = \frac{\eta_s}{\eta_p}. \quad (6)$$

Another dimensionless group that reflects elastic effects, is the Deborah number, De , which will be introduced later. The Nusselt number will also be introduced later, when steady convection is considered. Finally, two types of boundary conditions at the plates will be used in this study, namely, the *free-free* and *rigid-rigid* conditions. Only the former will be explicitly discussed in the formulation.

2.2. The two-dimensional problem

The problem is first examined in a two-dimensional (x, z) plane using a dynamical systems approach. In this case, it is convenient to introduce the stream function, $\psi(x, z, t)$, such that

$$u_x = -\psi_{,z}, \quad u_z = \psi_{,x}. \quad (7)$$

Upon elimination of the pressure, the conservation equations become

$$Pr^{-1}[\Delta\psi_{,t} + J(\psi, \Delta\psi)] = \frac{Rv}{Rv + 1} \Delta^2\psi + (\tau_{zz} - \tau_{xx})_{,xz} + \tau_{xz,xx} - \tau_{xz,zz} + \theta_{,x}, \quad (8)$$

$$\theta_{,t} + J(\psi, \theta) = \Delta\theta + Ra\psi_{,x}, \quad (9)$$

whereas the constitutive equation (5) leads to

$$E[\tau_{xx,t} + J(\psi, \tau_{xx}) + 2(\psi_{,xz} \tau_{xx} + \psi_{,zz} \tau_{xz})] = -\tau_{xx} - 2\psi_{,xz}/(Rv + 1), \quad (10a)$$

$$E[\tau_{zz,t} + J(\psi, \tau_{zz}) - 2(\psi_{,xx} \tau_{xz} + \psi_{,xz} \tau_{zz})] = -\tau_{zz} + 2\psi_{,xz}/(Rv + 1), \quad (10b)$$

$$E[\tau_{xz,t} + J(\psi, \tau_{xz}) - (\psi_{,xx} \tau_{xx} - \psi_{,zz} \tau_{zz})] = -\tau_{xz} + (\psi_{,xx} - \psi_{,zz})/(Rv + 1), \quad (10c)$$

where $J(\psi, \varphi) = \psi_{,x} \varphi_{,z} - \psi_{,z} \varphi_{,x}$ is the Jacobian operator in the variables ψ and φ . The thermal convection equations for a Newtonian fluid are recovered by taking the limit $Rv \rightarrow \infty$. This limit also corresponds to setting the relaxation and retardation times of the fluid equal (Bird *et al.* 1987).

Regardless of the nature of the boundaries, the temperature is fixed at the two plates at $z = \pm 1/2$, and the no-penetration condition holds, so that

$$\theta(x, z = -1/2, t) = \theta(x, z = +1/2, t) = 0, \quad (11)$$

$$\psi(x, z = -1/2, t) = \psi(x, z = +1/2, t) = 0. \quad (12)$$

For free-free conditions, the two plates are taken as stationary free surfaces so that the plates are stress free:

$$\tau_{xz}(x, z = \pm 1/2, t) + \frac{Rv}{Rv + 1} [\psi_{,xx}(x, z = \pm 1/2, t) - \psi_{,zz}(x, z = \pm 1/2, t)] = 0. \quad (13)$$

Initial conditions are obviously needed. However, their type and value are of little significance for the present problem since it is the long-term behaviour that is of interest.

It is important to observe that the Maxwell limit is recovered by setting $Rv = 0$ in equations (8) to (10). This limit corresponds to a polymer melt. The Newtonian flow is recovered in the limit $Rv \rightarrow \infty$ (or in the singular limit $E \rightarrow 0$), which is equivalent to setting $\eta_p = 0$. In this case, equations (10) admit the solution $\tau_{xx} = \tau_{zz} = \tau_{xz} = 0$, and equation (8) reduces to that corresponding to the RB convection of a Newtonian fluid (a solvent with viscosity η_s).

The normal stress terms in the constitutive equation are particularly well represented in the solution expansion. The Galerkin projection method is used to generate the dynamical system that governs the time-dependent coefficients. The truncation level is chosen on the basis of existing formulations for RB convection (Khayat 1994, 1995*a, b*, 1996) and Taylor–Couette flow (Khayat 1999) of viscoelastic fluids. An assessment of the convergence of the solution representation is also carried out. Unlike the critical Taylor number for the onset of stationary Taylor vortex flow, the critical Rayleigh number for the onset of stationary thermal convection is independent of fluid elasticity and viscosity ratio. This is due to the fact that the RB base solution is simply the origin in phase space, leading to the vanishing of the effect of the nonlinear terms in the linearization process around the conduction state. For this reason, a pre-critical range ($Ra < Ra_c^s$) and a post-critical range ($Ra > Ra_c^s$) are identified, similarly to Newtonian fluids. The onset of finite-amplitude overstability is examined for $Ra < Ra_c^s$. The influence of fluid elasticity, viscosity ratio and Prandtl number on the onset of stationary thermal convection is examined in the range $Ra > Ra_c^s$. The stability of the stationary solution branches is examined in detail.

The solution of equations (8) to (10) is carried out using the Galerkin projection method. The variables $\psi(x, z, t)$, $\theta(x, z, t)$ and $\tau_{ij}(x, z, t)$ are represented by infinite Fourier series of fundamental wavelength $2\pi/k$ (in units of D) in the x -direction, and complete sets of orthogonal functions satisfying the boundary conditions in the z -direction. Following McLaughlin & Martin (1975), the velocity, temperature and stress variables can be written as spectral sums:

$$\psi(x, z, t) = \sum_m \sum_n \psi_{mn}(t) e^{i(mkx + n\pi z)}, \quad (14a)$$

$$\theta(x, z, t) = i \sum_m \sum_n \theta_{mn}(t) e^{i(mkx + n\pi z)}, \quad (14b)$$

$$\tau_{ij}(x, z, t) = \sum_m \sum_n \tau_{ij}^{mn}(t) e^{i(mkx + n\pi z)}, \quad (14c)$$

where τ_{ij} represents τ_{xx} , τ_{xz} and τ_{zz} . Substitution of solution (14) into equations (8)–(10), and application of the Galerkin projection method, lead to an infinite set of coupled and nonlinear ordinary differential equations in the expansion coefficients ψ_{mn} , θ_{mn} and τ_{ij}^{mn} . The number of modes is reduced by invoking the symmetry allowed by equations (8)–(10) and the boundary conditions. It is not difficult to first infer from equations (8)–(10) and solutions (14) that the expansion coefficients can be taken to be real. This implies that the relations

$$\psi_{mn} = \psi_{-m-n}, \quad \theta_{mn} = -\theta_{-m-n}, \quad \tau_{ij}^{mn} = \tau_{ij}^{-m-n} \quad (15)$$

| | ψ_{11} | ψ_{13} | θ_{02} | θ_{11} | θ_{13} | τ_{xx}^{02} | τ_{xx}^{04} | τ_{xx}^{11} | τ_{xx}^{13} | τ_{zz}^{02} | τ_{zz}^{11} | τ_{zz}^{13} | τ_{xz}^{11} | τ_{xz}^{13} |
|-------|-------------|-------------|---------------|---------------|---------------|------------------|------------------|------------------|------------------|------------------|------------------|------------------|------------------|------------------|
| $M=6$ | × | | × | × | | | | × | | | × | | × | |
| 8 | × | | × | × | | × | | × | | × | × | | × | |
| 9 | × | × | × | × | | × | | × | | × | × | | × | |
| 10 | × | × | × | × | × | × | | × | | × | × | | × | |
| 11 | × | | × | × | | × | | × | × | × | × | × | × | × |
| 12 | × | × | × | × | × | × | | × | × | × | × | × | × | × |
| 13 | × | × | × | × | | × | × | × | × | × | × | × | × | × |
| 14 | × | × | × | × | × | × | × | × | × | × | × | × | × | × |

TABLE 1. Different truncation levels and corresponding modes included in modal assessment and convergence: an \times indicates that the mode is included.

must be satisfied. In addition, conditions (11) to (13) also imply that

$$\begin{pmatrix} \psi_{mn} \\ \theta_{mn} \\ \tau_{xz}^{mn} \end{pmatrix} = \begin{pmatrix} -\psi_{m-n} \\ -\theta_{m-n} \\ -\tau_{xz}^{m-n} \end{pmatrix} \quad n \text{ even}; \quad \begin{pmatrix} \psi_{mn} \\ \theta_{mn} \\ \tau_{xz}^{mn} \end{pmatrix} = \begin{pmatrix} \psi_{m-n} \\ \theta_{m-n} \\ \tau_{xz}^{m-n} \end{pmatrix} \quad n \text{ odd}. \quad (16)$$

There are no additional restrictions on the remaining stress components. Finally, conditions (15) and (16) give $\psi_{0n} = \tau_{xz}^{0n} = 0$.

A suitable level of truncation is imposed, which leads to the final nonlinear dynamical system. A judicious selection process is applied for the choice of the various modes in order to ensure the physical and mathematical coherence of the final model. Convergence assessment indicates that the qualitative flow is essentially the same as that based on the low-order description of previous works (Khayat 1994, 1995*a, b*). Quantitative convergence is secured when a number of modes similar to the one used for viscoelastic Taylor–Couette flow (Khayat 1997, 1999) is included. Table 1 displays the modes included for various levels of truncation, M being the total number of modes. For $M=6$, the equations can be reduced further to a 4-mode system, which, in the limit $Rv \rightarrow \infty$ reduces to the Lorenz equations (Khayat 1994, 1995*a*). The identification of the most dominant modes is not an obvious process in the present problem, given the simultaneous presence of both inertia and elastic normal stress effects. This process is guided by the accuracy of the steady-state solution as will be discussed shortly. It appears that the steady-state solution converges when $M > 12$. Therefore, all numerical results below are based on $M=13$, unless otherwise specified. An assessment of the influence of higher-order modes will be carried out below when the (non-trivial) steady-state branches are considered. However, the level $M=6$ has been used in the following preliminary discussion on the existence and stability of overstability, where analytical expressions can be recovered. Note that this level of truncation gives a reasonable qualitative picture.

2.3. The three-dimensional problem

An amplitude equation approach is used to assess the stability of three convection patterns, namely rolls, hexagons and squares, in the post-critical range, $Ra > Ra_c^*$. Readers are referred to Friedman (1956), Eckhaus (1965), Newell, Passot & Lega (1993), and Cross & Hohenberg (1993) for the general theory. The current derivation follows closely that developed by Parmentier *et al.* (2000), and is only briefly reviewed. The current amplitude equations are, however, obtained more accurately as certain terms dropped by Parmentier *et al.* (2000) are included here.

Equations (2) to (5) are written compactly as

$$NL(\mathbf{f}) = L_c(\mathbf{f}) + L_\Delta(\mathbf{f}), \tag{17}$$

where the super vector $\mathbf{f} = (\mathbf{u}, p, \theta, \tau)^T$. The explicit expressions of operators L_c and L_Δ are given, respectively, by

$$L_c = \begin{vmatrix} \frac{Rv}{Rv+1}\Delta & -\nabla & \mathbf{e}_z & \nabla \cdot \\ \nabla \cdot & 0 & 0 & 0 \\ Ra_c^s \mathbf{e}_z \cdot & 0 & \Delta & 0 \\ \frac{1}{Rv+1}\Gamma & 0 & 0 & -1 \end{vmatrix}, \tag{18}$$

$$L_\Delta = \begin{vmatrix} 0 & 0 & 0 & 0 \\ 0 & 0 & 0 & 0 \\ (Ra - Ra_c^s) \mathbf{e}_z \cdot & 0 & 0 & 0 \\ 0 & 0 & 0 & 0 \end{vmatrix}, \tag{19}$$

where Γ stands for the operator $\Gamma = \nabla(\cdot) + \nabla^T(\cdot)$, with, in particular, $\Gamma \mathbf{u} = \dot{\mathbf{y}}$. $NL(\mathbf{f})$ represents the nonlinear and the time-rate contributions, namely

$$NL(\mathbf{f}) = \begin{vmatrix} Pr^{-1}(\mathbf{u}_{,t} + \mathbf{u} \cdot \nabla \mathbf{u}) \\ 0 \\ \theta_{,t} + \mathbf{u} \cdot \nabla \theta \\ E[\tau_{,t} + \mathbf{u} \cdot \nabla \tau - (\nabla \mathbf{u})^T \cdot \tau - \tau \cdot \nabla \mathbf{u}] \end{vmatrix}. \tag{20}$$

The method of solution consists of expanding \mathbf{f} in terms of eigenfunctions of the linear problem in the form

$$\mathbf{f} = \sum_{p_1} \sum_{q_1} A_{q_1}^{p_1}(t) \mathbf{f}_{q_1}^{p_1}(x, y, z), \quad p_1 = 1, 2, \dots, \infty; \quad q_1 = \pm N, \dots, \pm 2, \pm 1. \tag{21}$$

The summation over q_1 extends on the N set of allowable wavevectors, \mathbf{k}_{q_1} , which in the case of an infinite horizontal extent can take all possible directions and moduli ($N \rightarrow \infty$), while the summation over p_1 runs over the whole set of eigenfunctions pertaining to a given wavevector \mathbf{k}_{q_1} . $A_{q_1}^{p_1}(t)$ designates the amplitude of the mode and must satisfy $\bar{A}_{q_1}^{p_1} = A_{-q_1}^{p_1}$ in order that \mathbf{f} be real; a bar over a symbol means complex conjugate. The eigenfunctions $\mathbf{f}_{q_1}^{p_1}(x, y, z)$ are solutions of the linear problems defined by

$$s_{q_1}^{p_1} M(\mathbf{f}_{q_1}^{p_1}(x, y, z)) = L_c(\mathbf{f}_{q_1}^{p_1}(x, y, z)), \tag{22}$$

where L_c is given by equation (18) while operator M is expressed by

$$M = \begin{vmatrix} Pr^{-1} & 0 & 0 & 0 \\ 0 & 0 & 0 & 0 \\ 0 & 0 & 1 & 0 \\ 0 & 0 & 0 & E \end{vmatrix}. \tag{23}$$

The eigenvalues, $s_{q_1}^{p_1}$, of the linear problem are ordered in such a way that $\text{Re}(s_{q_1}^1) > \text{Re}(s_{q_1}^2) > \dots > \text{Re}(s_{q_1}^n)$, where $\text{Re}(s)$ stands for the real part of s . Solutions $\mathbf{f}_{q_1}^{p_1}(x, y, z)$ are sought of the form

$$\mathbf{f}_{q_1}^{p_1}(x, y, z) = \mathbf{F}_{q_1}^{p_1}(z) \exp[i\mathbf{k}^{q_1} \cdot (\mathbf{e}_x x + \mathbf{e}_y y)], \tag{24}$$

where \mathbf{e}_x and \mathbf{e}_y are unit vectors in the x - and y -directions, respectively. $\mathbf{F}_{q_1}^{p_1}(z) = \{U_{q_1}^{p_1}(z), P_{q_1}^{p_1}(z), \Theta_{q_1}^{p_1}(z), \mathbf{T}_{q_1}^{p_1}(z)\}$, and is determined after substitution of expression (24) back into equation (22). The next step of the procedure consists of projecting the nonlinear equation (17) on the eigenfunctions $\mathbf{f}_{q_2}^{*p_2}(x, y, z)$ of the linear adjoint problem, which is formulated in Li (2003). This leads to

$$\langle NL(\mathbf{f}), \mathbf{f}_{q_2}^{*p_2}(x, y, z) \rangle = \langle L_c(\mathbf{f}), \mathbf{f}_{q_2}^{*p_2}(x, y, z) \rangle + \langle L_\Delta(\mathbf{f}), \mathbf{f}_{q_2}^{*p_2}(x, y, z) \rangle. \quad (25)$$

Here an angle bracket denotes the average integral of the scalar product defined by

$$\langle a, b \rangle \equiv \lim_{L \rightarrow \infty} \frac{1}{4L^2} \int_v P_v(a, b) \, dx dy dz, \quad (26)$$

where P_v is scalar product defined on the volume v . Equation (25) stands for an infinite number of ordinary differential equations for the unknown amplitudes $A_{q_1}^{p_1}(t)$. After integration by parts and using relation (22), we are led to the infinite sequence of amplitude equations

$$\begin{aligned} A_{q_1}^{p_1, t} C_0(q_1, p_1) &= s_{q_1}^{p_1} C_0(q_1, p_1) A_{q_1}^{p_1} + (r - 1) \sum_{p_2}^{\infty} C_1(q_1, p_1, p_2) A_{q_1}^{p_2} \\ &\quad - \sum_{p_2, p_3}^{\infty} \sum_{q_2, q_3} \delta(\mathbf{k}^{-q_1} \mathbf{k}^{q_2} \mathbf{k}^{q_3}) C_2 \left(\begin{matrix} p_1, & p_2, & p_3 \\ q_1, & q_2, & q_3 \end{matrix} \right) A_{q_2}^{p_2} A_{q_3}^{p_3}, \end{aligned} \quad (27)$$

where $r = Ra/Ra_c^s$ is the reduced Rayleigh number, which will be used as the control parameter instead of Ra . The δ function is defined by

$$\delta(\mathbf{k}^{-p_1} \mathbf{k}^{p_2} \mathbf{k}^{p_3}) = \begin{cases} 0, & \mathbf{k}^{-p_1} + \mathbf{k}^{p_2} + \mathbf{k}^{p_3} \neq 0 \\ 1, & \mathbf{k}^{-p_1} + \mathbf{k}^{p_2} + \mathbf{k}^{p_3} = 0 \end{cases}$$

The coefficients C_0 , C_1 , and C_2 are reported in Li (2003).

It is, of course, highly desirable to reduce the infinite number of nonlinear coupled ordinary differential equations to a finite set of equations. This will be achieved by separating the set of eigenmodes $\mathbf{f}_{q_1}^{p_1}(x, y, z)$ into two subsets K_c and K_s . The subset K_c contains the critical eigenmodes with a zero growth rate ($Re(s_{q_1}^{p_1}) = 0$). The critical eigenmodes are the ones corresponding to $p_1 = 1$ and $|k_{q_1}| = k_c^s$, with k_c^s being the critical wavenumber at the onset of stationary convection (see below). Since the stability of hexagonal, square and roll cells is studied, one need only consider the twelve wave vectors $k_{q_1}(q_1 = \pm 1, \pm 2, \dots, \pm 6)$ distributed on a circumference of radius k_c^s and making an angle of 30° between each other (see figure 6 in Parmentier *et al.* 2000). It follows that the twelve critical eigenmodes are $\mathbf{f}_{q_1}^1(x, y, z)$, $q_1 = \pm 1, \pm 2, \dots, \pm 6$. The subset K_s consists of all stable eigenmodes characterized by a negative growth rate ($Re(s_{q_1}^{p_1}) < 0$). In a weakly nonlinear regime, these stable eigenmodes are rapidly relaxing, from which it follows that the amplitudes in equation (27) corresponding to these stable modes can be notably simplified. It is justified to drop the term in the equation (27) containing the time derivative because these modes are quickly damped. Thus, the following relation between the stable and the critical modes is obtained:

$$\begin{aligned} A_{q_1}^{p_1} &= -(r - 1) C_1(q_2, 1, 1) A_{q_2}^1 + \frac{1}{s_{q_1}^{p_1} C_0(q_1, p_1)} \sum_{q_2, q_3} \delta(\mathbf{k}^{-q_1} \mathbf{k}^{q_2} \mathbf{k}^{q_3}) C_2 \left(\begin{matrix} p_1, & 1, & 1 \\ q_1, & q_2, & q_3 \end{matrix} \right) A_{q_2}^1 A_{q_3}^1, \\ &\quad q_2, q_3 = \pm 1, \pm 2, \dots, \pm 6. \end{aligned} \quad (28)$$

Note that the first term on the right-hand side is not accounted for in the formulation of Parmentier *et al.* (2000). It follows from the above consideration that the infinite number of ordinary differential equations (27) reduces to a finite number of equations, namely

$$A_{q_1}^{p_1}, C_0(q_1, 1) = (r - 1) \sum_{p_2}^{\infty} C_1(q_1, 1, p_2) A_{q_1}^{p_2} - \sum_{p_2, p_3}^{\infty} \sum_{q_2, q_3} \delta(\mathbf{k}^{-q_1} \mathbf{k}^{q_2} \mathbf{k}^{q_3}) C_2 \left(\begin{matrix} 1, & p_2, & p_3 \\ q_1, & q_2, & q_3 \end{matrix} \right) A_{q_2}^{p_2} A_{q_3}^{p_3}, \quad q_1 = \pm 1, \pm 2, \dots, \pm 6. \quad (29)$$

The number of modes p_2, p_3 is increased until a relative accuracy is reached. After substitution of equation (28) into equation (29) and omitting terms of order higher than three (this is justified as one remains in the weakly nonlinear regime), the following amplitude equations are obtained,

$$\tau_0 \frac{dA_1}{dt} = (r - 1)A_1 - b(|A_2|^2 + |A_3|^2)A_1 - c|A_1|^2 A_1 - d(|A_6|^2 + |A_5|^2)A_1 - e|A_4|^2 A_1, \quad (30)$$

$$\tau_0 \frac{dA_2}{dt} = (r - 1)A_2 - b(|A_1|^2 + |A_3|^2)A_2 - c|A_2|^2 A_2 - d(|A_4|^2 + |A_6|^2)A_2 - e|A_5|^2 A_2, \quad (31)$$

$$\tau_0 \frac{dA_3}{dt} = (r - 1)A_3 - b(|A_1|^2 + |A_2|^2)A_3 - c|A_3|^2 A_3 - d(|A_4|^2 + |A_5|^2)A_3 - e|A_6|^2 A_3, \quad (32)$$

$$\tau_0 \frac{dA_4}{dt} = (r - 1)A_4 - b(|A_5|^2 + |A_6|^2)A_4 - c|A_4|^2 A_4 - d(|A_2|^2 + |A_3|^2)A_4 - e|A_1|^2 A_4, \quad (33)$$

$$\tau_0 \frac{dA_5}{dt} = (r - 1)A_5 - b(|A_4|^2 + |A_6|^2)A_5 - c|A_5|^2 A_5 - d(|A_1|^2 + |A_3|^2)A_5 - e|A_2|^2 A_5, \quad (34)$$

$$\tau_0 \frac{dA_6}{dt} = (r - 1)A_6 - b(|A_4|^2 + |A_5|^2)A_6 - c|A_6|^2 A_6 - d(|A_1|^2 + |A_2|^2)A_6 - e|A_3|^2 A_6. \quad (35)$$

Here, τ_0 , the relaxation time, and the coefficients b, c, d , and e depend generally on Pr, Rv, E and r , and are given explicitly in Li (2003). Equations (30) to (35) are usually referred to as the Landau equations (Drazin & Reid 1981). Note that the superscripts have been omitted since all of them are equal to one.

3. Review of the linear stability picture

Although the current work is focused on the nonlinear range, a review of the linear stability picture is helpful for purposes of reference and coherence in notation. For a comprehensive account of linear stability analysis see (Lason 1992). For a small value of E or large value of Rv , one expects the behaviour of the flow to be similar to the Newtonian regime, at least around the purely conductive state. Similarly to the case of a Newtonian fluid, one of the steady-state solution branches corresponds to pure heat conduction. When Ra exceeds a critical value, Ra_c^s , the heat conduction state loses its stability to stationary convection. In contrast to Newtonian fluids, which admit only rolls in the post-critical range, convection patterns of viscoelastic fluids can be in the form of rolls or hexagons depending on the level of elasticity (see below). The value of Ra_c^s is independent of E or Rv because the base state in this case is the same for both

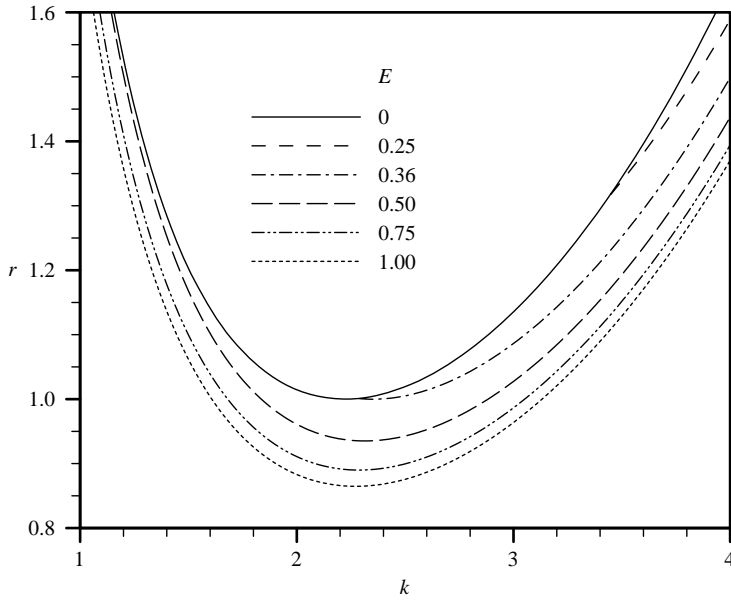


FIGURE 1. Plots of the marginal stability curves on (r, k) -planes for different elasticity number with $Pr = 7$ and $Rv = 3.75$.

Newtonian and non-Newtonian fluids since it corresponds to pure conduction. This is in contrast to viscoelastic Taylor–Couette flow, where the base flow depends on E and Rv , thus leading to critical conditions that are influenced by elastic effects. As E increases, however, the stability picture changes, giving rise to elastic overstability. The stability of weakly and strongly elastic fluids will be examined.

3.1. Loss of stability of the conductive state for weakly and strongly elastic fluids

It is helpful to first review the results of the linear stability analysis of the conductive state. For this purpose, it is much more illuminating to restrict the analysis to the dominant modes as in previous studies (Khayat 1994, 1995a, b). Thus, the truncation level will be restricted to $M = 6$ in §§ 3.1 and 3.2. It is not difficult to establish, as in the case of a Newtonian fluid, that the value of the Rayleigh number for the onset of stationary convection is equal to $(\pi^2 + k^2)^3/k^2$ for the most dominant mode. The critical (smallest) Rayleigh number and the corresponding wavenumber are equal to $Ra_c^s = 657.51$ and $k_c^s = 2.221$, respectively.

Linear stability analysis around the conduction state leads to the following characteristic equation:

$$\sigma^3 + \left(\frac{Rv}{Rv+1} Pr + \frac{1}{(k^2 + \pi^2)E} + 1 \right) \sigma^2 + \left(\frac{Rv}{Rv+1} Pr + \frac{Pr+1}{(k^2 + \pi^2)E} - r \frac{Pr k^2 Ra_c^s}{(k^2 + \pi^2)^3} \right) \sigma + \frac{Pr}{(k^2 + \pi^2)E} \left(1 - r \frac{k^2 Ra_c^s}{(k^2 + \pi^2)^3} \right) = 0, \quad (36)$$

where σ is the complex eigenvalue. The derivation of equation (36) and its counterpart for rigid–rigid boundary conditions is given in Li (2003). Some typical marginal stability curves for several values of E are illustrated in figure 1, with $Pr = 7$ and $Rv = 3.75$. The value of $Rv = 3.75$ is typical of the viscosity ratio for Boger fluids,

which obey the Oldroyd-B constitutive equation (Walters 1980; Bird *et al.* 1987; Muller, Shaqfeh & Larson 1993). The solid curve is the marginal stability curve for Newtonian fluids, and is independent of Pr . In this case, there is an exchange of stability between the pure conduction state and stationary convection. The non-solid curves correspond to the marginal stability for oscillatory convection (overstability).

Two regimes are clearly distinguishable from figure 1. The weakly elastic regime, which is taken to correspond to $E < E^h$, where E^h is the level of elasticity below which stationary convection is first observed (in this case $E^h = 0.362$). In this regime, however, oscillatory convection is still possible for a range of wavenumbers corresponding to $k > k^i$ (the point at which the solid and non-solid curves intersect). The strongly elastic regime corresponds to $E > E^h$, where oscillatory convection is predicted to be observed first. In this case, the conductive state loses its stability to oscillatory convection at a Rayleigh number that is smaller than Ra_c^s . It is thus appropriate to define a weakly (strongly) elastic fluid, as a fluid for which $E < E^h$ ($E > E^h$). Note that the critical wavenumber corresponding to the onset of oscillatory convection is always larger than k_c^s . Thus, the convective pattern becomes increasingly difficult to detect for the more elastic fluids. This prediction is in agreement with Martínez-Mardones & Pérez-García (1990). In the strongly elastic regime, stationary convection remains possible for a range of k values ($k < k^i$) that diminishes as E increases. Above a certain elasticity level (here $E > 0.553$), only oscillatory convection is predicted for any wavenumber.

The dependence of the critical elasticity number, E^h , corresponding wavenumber, k^h , and oscillation frequency, f^h , on the Prandtl number is plotted in figure 2 for different levels of the viscosity ratio. Both the low and high ranges of Pr values are examined in an attempt to cover a wide range of viscoelastic fluids. In this regard, rarefied gases ($Pr \ll 1$) display a strong viscoelastic character (see Khayat & Eu 1989 and references therein). It turns out that for most polymeric fluids of practical interest ($Pr \gg 1$), k^h depends very weakly on the fluid parameters Pr and Rv . The figure indicates that fluids with higher thermometric conductivity (smaller Pr) are less likely to exhibit oscillatory convection, which sets in at a relatively high elasticity level, and is difficult to detect in practice given the low oscillation frequency. However, for typical polymeric solutions ($Pr \gg 1$), the influence of fluid conductivity is less significant as indicated by the flattening of the curves at larger value of Pr , especially for non-Maxwell fluids. Thus it is the viscosity ratio of the polymeric solution that determines the likelihood for steady or oscillatory convective motion. It is observed that k^h is larger than k_c^s and decreases asymptotically to the Newtonian limit, k_c^s , with increasing Rv for any Pr . Although E^h increases linearly with Rv , both k^h and f^h experience a significant drop as Rv increases from zero. Both the wavenumber and frequency increase indefinitely with Pr in the case of a Maxwell fluid. This indicates that the thermal convection for polymeric melts tends to set in with a much larger frequency and smaller cell size than for polymeric solution. Note finally that the Newtonian limit ($Rv \rightarrow \infty$) is recovered as $E^h \rightarrow \infty$, $k^h \rightarrow k_c^s$ and $f^h \rightarrow 0$. It is interesting to observe from figure 2 that there seems to be a minimum elasticity level, $E \approx 0.03$, for any Pr and Rv values, below which no overstability is possible.

3.2. Overstability for strongly elastic fluids

The onset of overstability coincides with the emergence of a pair of imaginary eigenvalues in the characteristic equation (36). Thus, it can be deduced that the

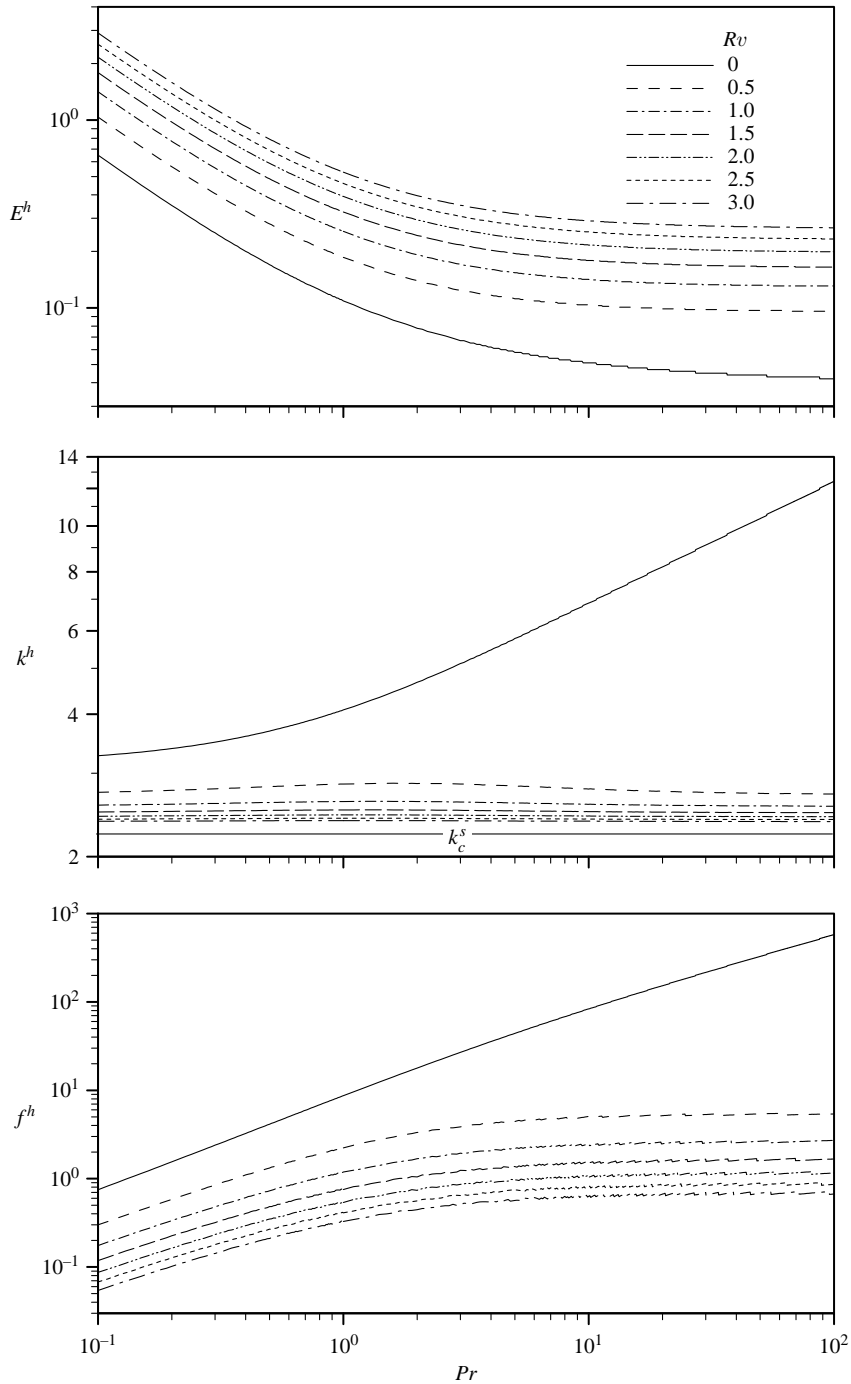


FIGURE 2. Influence of the Prandtl number on the critical elasticity number, E^h , the corresponding wavenumber, k^h , and the oscillation frequency, f^h , for the onset of oscillatory convection. The curves are shown for $Rv \in [0, 3]$.

reduced Rayleigh number for the onset of oscillatory convection is given by

$$r^h = \frac{(k^2 + \pi^2)^3 \left(RvPr + \frac{Rv + 1}{(k^2 + \pi^2)E} \right) \left[RvPr + \left(\frac{Pr + 1}{(k^2 + \pi^2)E} + 1 \right) (Rv + 1) \right]}{(RvPr + Rv + 1)(Rv + 1)Prk^2Ra_c^s}. \quad (37)$$

Oscillatory convection (overstability) always emerges for strongly elastic fluids ($E > E^h$) at a critical Rayleigh number Ra_c^h smaller than Ra_c^s , or $r_c^h = Ra_c^h/Ra_c^s < 1$. The r_c^h is the minimum value of r^h and is obtained numerically. The conductive state remains unconditionally stable for $r < r_c^h$, and becomes overstable for $r > r_c^h$.

The initial frequency of oscillation is given by Khayat (1995a, b):

$$f = \frac{1}{E} \sqrt{\frac{(k^2 + \pi^2)EPr - (Pr - 1)(Rv + 1)}{PrRv + Rv + 1}}. \quad (38)$$

The critical reduced Rayleigh number, r_c^h , for the onset of overstability generally decreases with E (Martínez-Mardones & Pérez-García 1992). It is not difficult to show from equation (37) that r_c^h tends asymptotically to $Rv(k^2 + \pi^2)^3/[(Rv + 1)k^2Ra_c^s]$ in the limit $E \rightarrow \infty$. If E is substituted by E^h in equation (37), one obtains the important result for r_c^h ,

$$r_c^h(E = E^h) = 1, \quad (39)$$

which indicates that there cannot be a stability exchange between the conductive state and oscillatory convection when $r > 1$. This does not mean, however, that an overstable solution cannot exist for $r > 1$. Equation (39) also indicates that a point exists where the three phases: pure conduction, stationary and oscillatory convection coexist (Brand & Zielinska 1986). The influence of the viscosity ratio on the onset of overstability is shown in figure 3 for $Pr = 7$, where the critical reduced Rayleigh number, r_c^h , the corresponding wavenumber, k_c^h , and frequency, f_c^h , for the onset of overstability are plotted against E for $Rv \in [0, 3.75]$. Both r_c^h and k_c^h generally decrease with E . The corresponding frequency, f_c^h , displays generally a maximum that tends to occur at larger E as Rv increases. The overall frequency decreases with viscosity ratio. There is a sharp drop in the frequency as Rv exceeds zero. In addition, there is a jump in frequency (from zero), which occurs at the critical elasticity number, E^h .

The influence of the Prandtl number on the onset of overstability is shown in figure 4 for $Rv = 0.5$, where the critical reduced Rayleigh number, r_c^h , the corresponding wavenumber, k_c^h , and frequency, f_c^h , for the onset of overstability are obtained numerically and plotted against E . The figure indicates that the region for elastic overstability grows as Pr increases. This observation is in agreement with the results of Brand & Zielinska (1986) in the case of a Maxwell fluid. At large Pr values ($Pr > 10$), as is typically the case of polymeric solutions, the region of overstability remains essentially unchanged, as indicated by the saturation of the curves in the figure, especially those corresponding to the critical Rayleigh number and wavenumber. It is thus possible to obtain more explicit relations by taking the limit of infinite Pr of equations (37) and (38), which for a Maxwell fluid gives

$$\lim_{Pr \rightarrow \infty} r_c^h = \frac{4\pi^2}{E} \quad \text{and} \quad \lim_{Pr \rightarrow \infty} k_c^h = \pi,$$

a result that is in agreement with Eltayeb (1977). In this case, the oscillation frequency becomes infinite.

Rigid–rigid boundary conditions were also investigated previously (Martínez-Mardones & Pérez-García 1990; Martínez-Mardones *et al.* 1996; Li 2003). It was

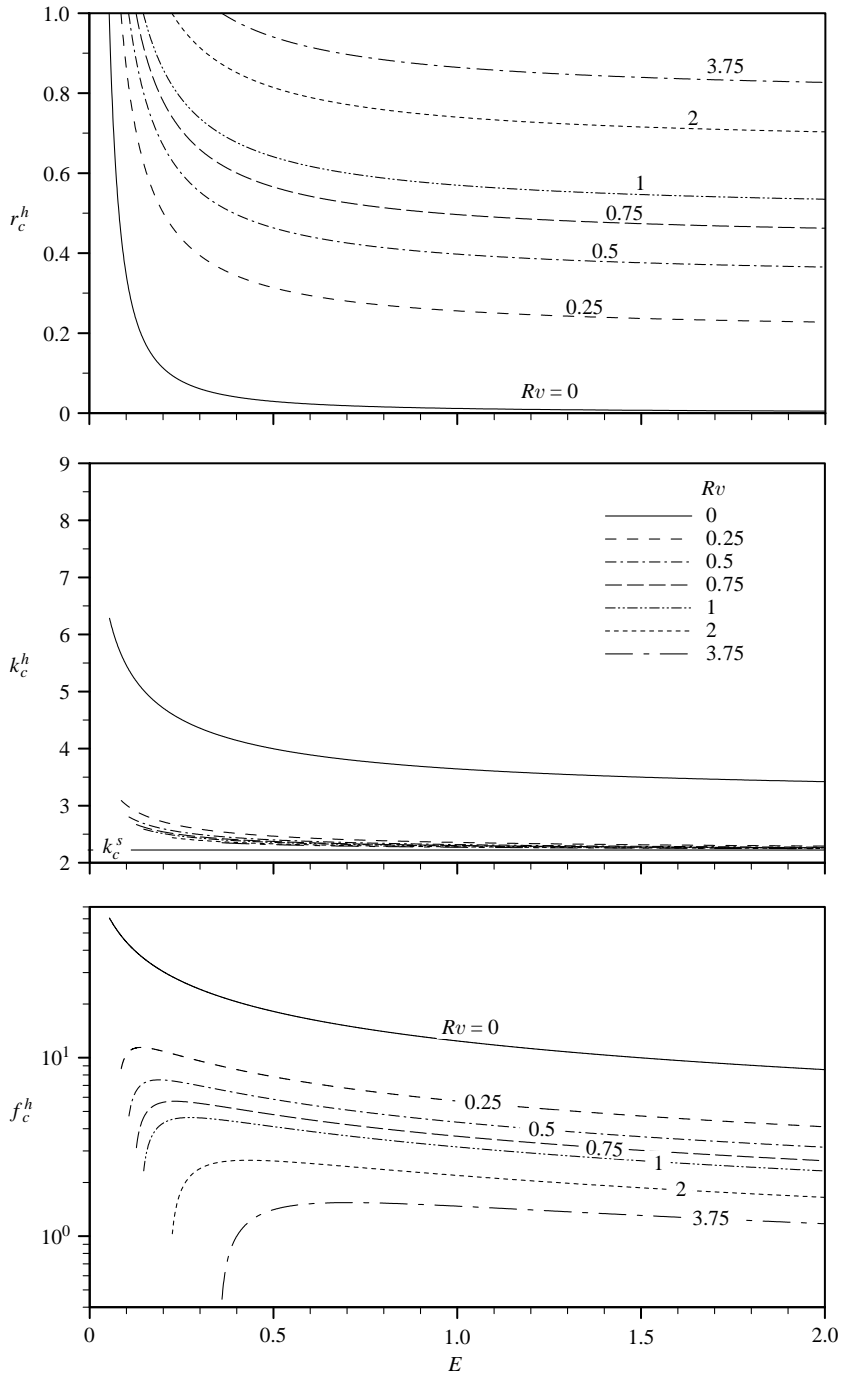


FIGURE 3. Influence of the viscosity ratio on the reduced critical Rayleigh number, r_c^h , the corresponding wavenumber, k_c^h , and the oscillation frequency f_c^h , for the onset of overstability from the conductive state. The curves are shown for $Rv \in [0, 3.75]$ and $Pr = 7$.

found that the type of boundaries not only has no influence on the qualitative behaviour, but also leads to little quantitative difference, especially at high elasticity number.

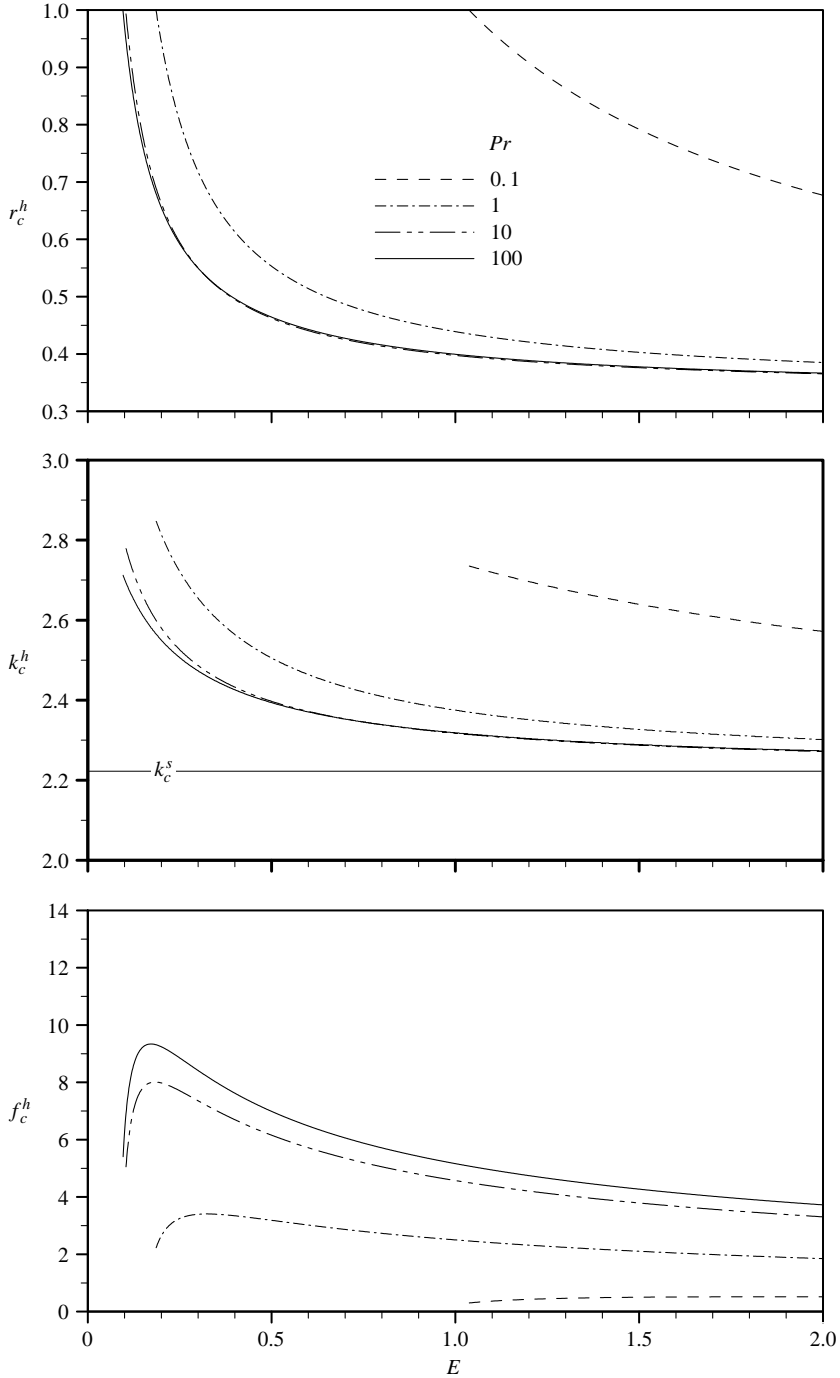


FIGURE 4. Influence of the Prandtl number on the reduced critical Rayleigh number, r_c^h , the corresponding wavenumber, k_c^h , and the oscillation frequency f_c^h , for the onset of overstability from the conductive state. The curves are shown for $Rv = 0.5$.

The onset of overstability appears to be enhanced the more elastic the fluid is, and is more difficult to achieve for fluids with significant retardation time or that are highly (heat) conductive. The existence of an elastic overstable mode for strongly elastic

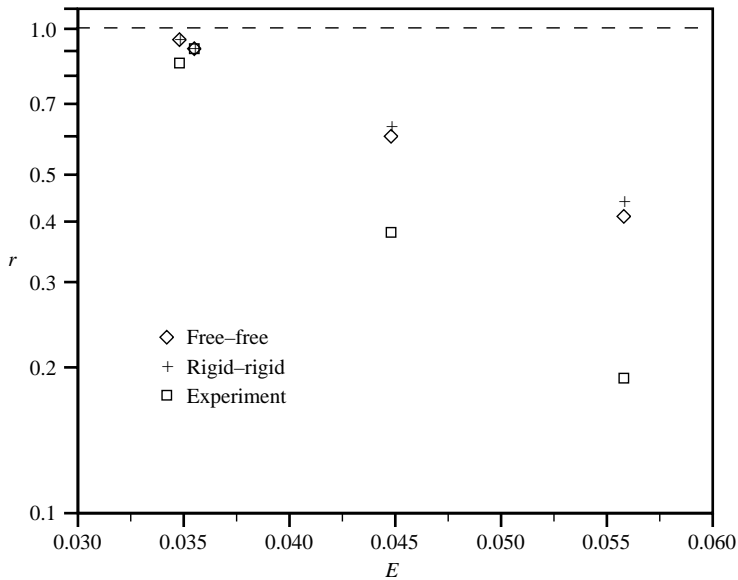


FIGURE 5. Comparison between theory and experiment (Kolodner 1998) for the reduced Rayleigh number at the onset of oscillatory convection as function of elasticity number.

fluids predicted by linear stability analysis has been confirmed by the experimental measurements of Kolodner (1998), who examined the thermal convection of DNA suspensions in a narrow annular configuration. Most experimental results focused on the conditions for the onset of the elastic overstable mode. Travelling short rolls (indicating oscillatory thermal convection) are observed at Rayleigh number smaller than Ra_c^s for DNA suspensions with sufficiently large elasticity number. Although a direct comparison cannot be carried out between the present calculations and the experiment, a qualitative comparison remains possible. The fluids used in the experiment were suspensions of T2 bacteriophage DNA in a weak aqueous buffer. The relevant parameters, namely, E , Rv and Pr were provided from the experiment (see tables 2 and 3 in Kolodner 1998).

Comparison between theory and experiment is shown in figure 5, where the critical reduced Rayleigh number, r , for the onset of oscillatory convection is plotted against E . Results based on both the free–free and rigid–rigid formulations are included. The threshold for the onset of oscillations is a decreasing function of E , dropping below the threshold for the onset of stationary convection at $E = 0.031$. The theoretical predictions tend to overestimate the critical Rayleigh number, especially in the higher elasticity range. Comparison of the critical oscillation frequencies leads to no agreement with experiment. This discrepancy was also noted by Kolodner (1998) who attributed it to the inadequacy of existing constitutive models, which do not account for the transport of DNA molecules by the flow and their accumulation at stagnation points. However, in such cases, the cause of the onset of oscillatory convection is still the elasticity of the fluid, but the time scales of the oscillations have as much or more to do with solute diffusion than with elasticity.

4. Finite-amplitude thermal convection and pattern selection

In this section, the influence of fluid elasticity and viscosity ratio on the onset and stability of finite-amplitude thermal convection is examined in the presence of inertia. While the pre-critical range $Ra < Ra_c^s$ ($r < 1$) is identified as the elastic range, given

the relative dominance of normal stress effects, the range $r > 1$ will be identified as the elasto-inertial range. The emergence of finite-amplitude oscillatory convection will be examined first. The important issue of pattern selection will then be examined in some detail.

4.1. Finite-amplitude oscillatory convection

Elastic overstability has only been observed in the RB convection of polymeric fluids (Kolodner 1998). However, in general, there is little experimental data regarding the thermal convection of viscoelastic fluids. On the other hand, purely elastic oscillating vortices have been observed in Taylor–Couette flow (Muller *et al.* 1993). Measurements of the axial velocity component indicate that, at a critical elasticity number, E^h say, the flow field undergoes transition from the purely azimuthal flow to a time-dependent (oscillatory) flow. For $E > E^h$, higher harmonics appear in the density power spectrum of the velocity signal. The value of Re imposed is deliberately small to ensure that no inertia-driven Taylor vortices arise, so that the oscillatory cell structure may be attributed to fluid elasticity. The similarity between the RB convection and TCF suggests that the mechanism for overstability may be common to both flow contexts. In the present work, however, inertia plays an important role in the analysis as its influence on the emergence of elastic overstability is examined. It was shown above that, at $E = E^h$ (for given r), the fluid undergoes a transition from the purely conduction state to time-periodic flow at a Rayleigh number below the critical value Ra_c^s , with the latter corresponding to the onset of stationary convection. The emergence of higher harmonics is a nonlinear phenomenon, and therefore can only be confirmed through numerical calculation. In the experiments of Muller *et al.* (1993), there is a loss of periodicity as the elasticity number increases, leading, eventually, to aperiodic motion. A similar phenomenon occurs here that is important to examine in some detail.

The emergence of oscillatory rolls is now examined for a fluid with $Rv = 0.5$ and $Pr = 7$. The value of r is fixed at 0.6, which is low enough for elastic normal stress effects to be dominant. The control parameter is the elasticity number, E . In this case, linear stability analysis suggests that the value of the critical elasticity number for the onset of the oscillatory convection is equal to $E^h = 0.26$. For $E < E^h$, the conductive state is unconditionally stable. The solution decays oscillatorily to the origin (in phase space). As E slightly exceeds 0.26, the solution is attracted to and locked on a periodic orbit. The influence of fluid elasticity on the motion is examined for the range $0.27 < E < 0.7$. The motion is assessed in figures 6 and 7, by inspecting the time signature and the power density spectrum for the Nusselt number. The Nusselt number is defined in terms of the heat flux, Q , at the lower plate, averaged over a cell width:

$$Nu = \frac{\langle Q(x, z = -1/2, t) \rangle D}{K\delta T} = 1 - \frac{1}{Ra} \langle \theta_{,z}(x, z = -1/2, t) \rangle = 1 + \frac{2\pi}{Ra} \theta_{02}, \quad (40)$$

where $\langle \rangle$ denotes integration over $x \in [0, 2\pi/k]$.

For $0.27 < E < 0.61$, the time signature shows a periodic motion similar to the (linear) harmonic oscillator with the amplitude of the signal increasing with E . At $E = 0.3$, the motion remains periodic. The corresponding power spectrum indicates the presence of a dominant (dimensionless) frequency at $f_1 = 2.32$ that tends to increase slowly with E . There is an even harmonic that is present in the power spectrum. The number of harmonics increases with E ; both even and odd harmonics are present. For $E > 0.61$, the periodic regime in turn loses its stability, to be replaced by a

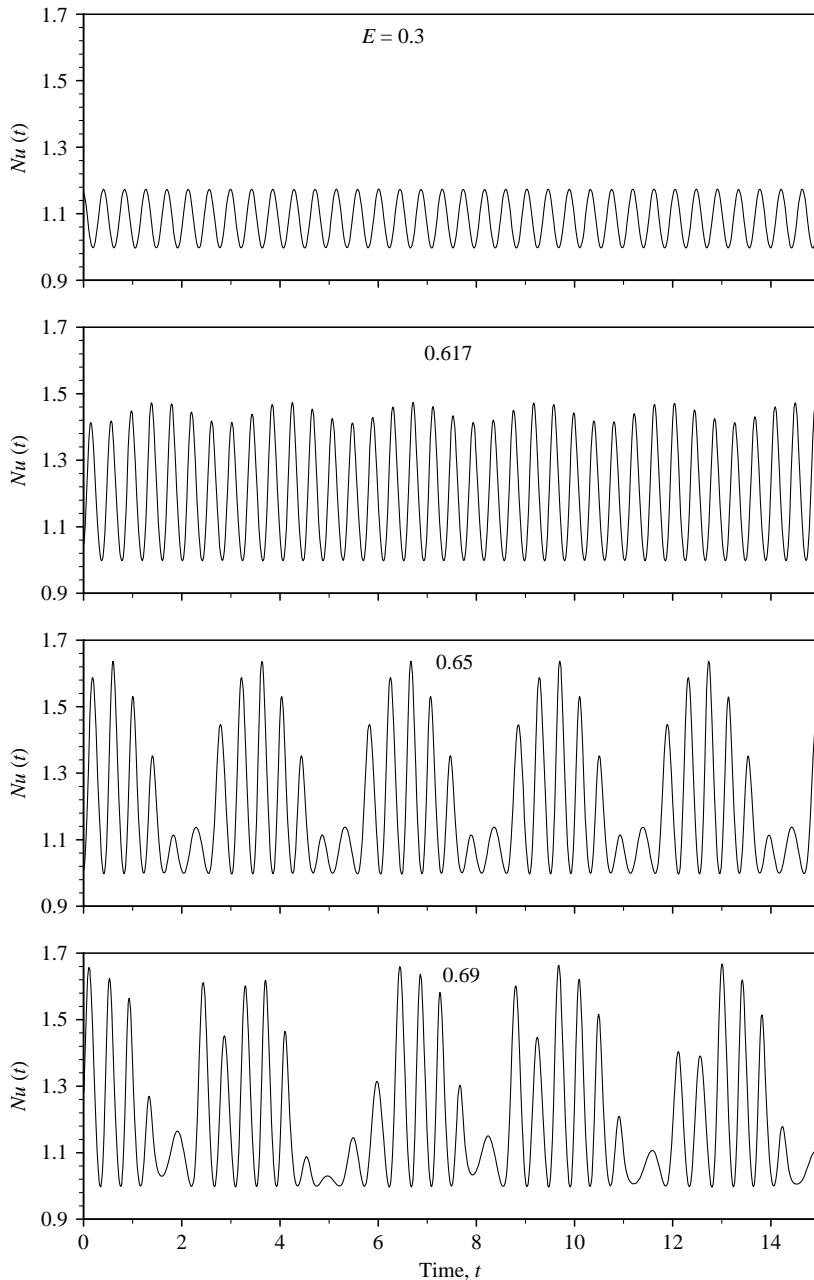


FIGURE 6. Oscillatory convection in the pre-critical range ($r=0.6$). Time signature for the Nusselt number, Nu , and influence of fluid elasticity for the range $E \in [0.3, 0.7]$, for a fluid with $Rv=0.5$ and $Pr=7$.

quasi-periodic regime with two fundamental frequencies. Typical behaviour is illustrated in figures 6 and 7 for $E=0.617$. The Nusselt number now clearly shows a strong modulation in the signal that is typical of quasi-periodic behaviour, and is clearly evident from the power spectrum. It is observed that the fundamental frequency has slightly increased, to $f_1=2.436$, with two additional even higher

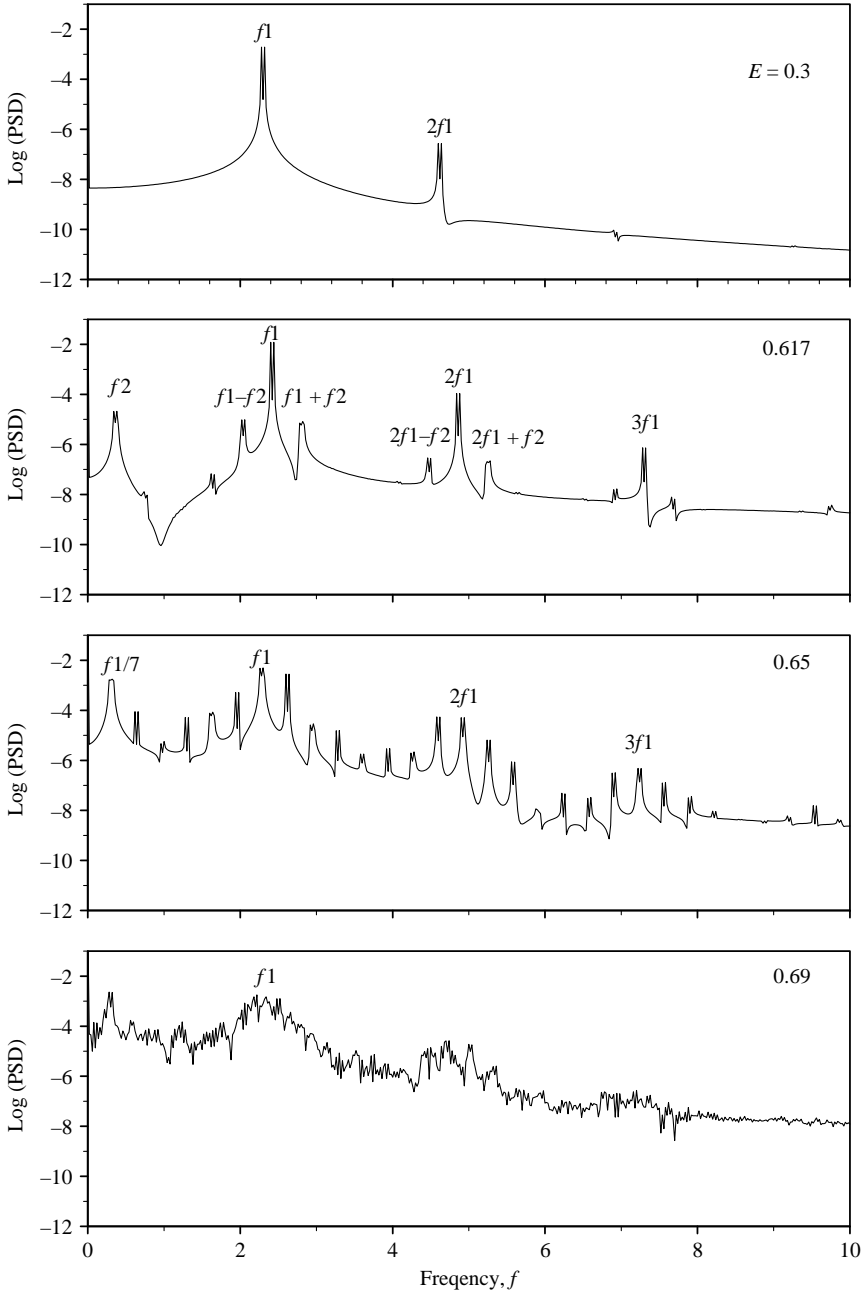


FIGURE 7. Oscillatory convection in the pre-critical range ($r=0.6$). Power density spectrum for the Nusselt number, and influence of fluid elasticity for the range $E \in [0.3, 0.66]$, for a fluid with $Rv = 0.5$ and $Pr = 7$.

harmonics appearing at $2f_1$ and $4f_1$. The power spectrum shows the emergence of a second dominant frequency at $f_2 = 0.384$. This is a definitely quasi-periodic regime with two dominant incommensurate frequencies and their harmonics. Note that the power spectral density is plotted logarithmically against the dimensionless frequency.

Some of the frequencies are clearly identified in the spectrum in figure 7 for $E = 0.617$. The frequency of each line is indexed by $f = m_1 f_1 + m_2 f_2$, where m_1 and m_2 are integers.

The two-frequency quasi-periodic convection persists as the elasticity number is further increased. The time signature of the Nusselt number shows additional modulation. At this stage, one expects that a further increase in E should eventually lead to chaotic behaviour, via, most likely, the emergence of a third incommensurate frequency, f_3 . This, of course, would have been the Ruelle–Takens–Newhouse (RTN) scenario (Newhouse, Ruelle & Takens 1978), which consists of a total of three successive Hopf bifurcations that occur, producing three frequencies, f_1 , f_2 and f_3 . Then according to RTN, the corresponding torus T^3 can, under fairly general conditions, become unstable and be replaced by a strange attractor. The time-dependent signal would no longer have been quasi-periodic with three frequencies, but chaotic. However, despite the plausibility of the RTN scenario, this is not what is found here when the level of fluid elasticity is further increased.

As E is further increased, making nonlinear effects more important, there is a frequency locking of order seven that becomes evident from the time signature, as illustrated typically for $E = 0.65$. The tendency toward frequency locking can, to some extent, be inferred from figure 7 for $E = 0.617$. From a physical point of view, this means that the frequencies f_1 and f_2 of the quasi-periodic regime encountered at the lower elasticity numbers are now commensurate: $f_1/f_2 = 7$ ($f_1 = 2.31$ and $f_2 = 0.33$). The Nusselt number exhibits severe periodic decrease of convective heat transport, corresponding to the depressed parts of the time signal in figure 6 for $E = 0.65$.

Frequency locking exists for $0.63 < E < 0.68$. Just above $E = 0.68$, there is again loss of periodicity, and the dimension of the phase orbit is no longer one, but is part of a strange attractor. That is, the torus T^2 has been destroyed, as reflected in the chaotic time signature, and, more evidently, the broadening of the base in the power spectrum that is shown for $E = 0.69$. The trace of the two previous frequencies remains observable at $f_1 = 2.28$ and $f_2 = 0.31$, which obviously shows that the two frequencies are, once again, incommensurate. Unlike the RTN route to chaos through which a torus T^3 is transformed into a strange attractor, the present scenario follows the Curry–Yorke model (Curry & Yorke 1977). In this case, chaos appears directly from a quasi-periodic regime with two frequencies (i.e. without the appearance of a third frequency). In other words, the route corresponds to the destabilization, or the destruction, of a T^2 torus. There is no incompatibility between the destabilization of T^2 and the reasoning behind the RTN scenario, which conjectures that T^3 has the minimum dimension required for a strange attractor to appear. Indeed, in the present problem, if chaos arises starting from T^2 , it is due to the manifestation of another degree of freedom, not in the form of a third frequency, but by the gradual departure of the trajectories from T^2 , which amounts to the destruction of the torus. The Curry–Yorke scenario remains qualitatively unchanged when more modes are added. Only the value of the elasticity number at each transition stage is affected. For instance, when 100 modes are used, chaos is found to set in at $E = 0.4$ instead of 0.68 when only 13 modes are used. It should also be noted that real systems typically exhibit spatial modulation in geometry or flow conditions (Kelly & Pal 1978). In this case, the scenario predicted in figures 6 and 7 should be interpreted with some caution. For instance, it is well known that boundary modulation leads to a smooth bifurcation as opposed to the supercritical or Hopf bifurcation predicted in the current ideal system. The ensuing post-critical behaviour is expected to be altered.

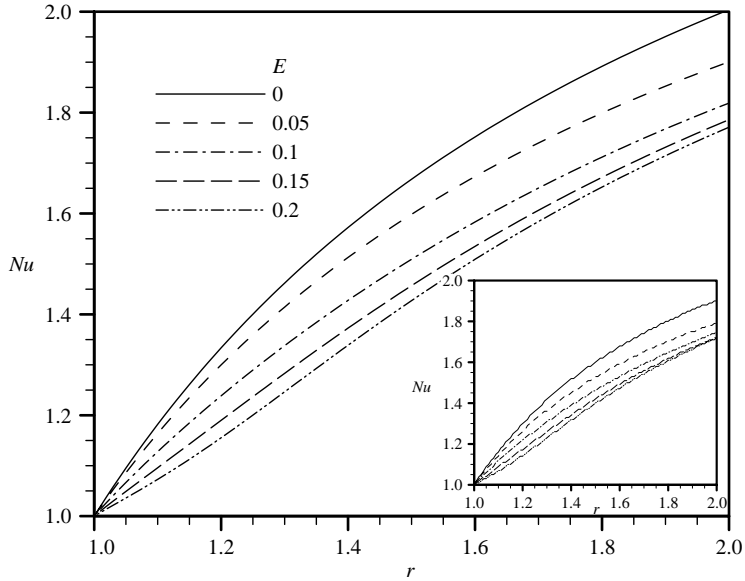


FIGURE 8. Bifurcation diagrams and influence of elasticity on stationary thermal convection. Nusselt number is plotted against the reduced Rayleigh number r for $E \in [0, 0.2]$ with $Rv = 3.75$ and $Pr = 7$. Inset shows the comparison with the solutions obtained with amplitude equation method.

4.2. Influence of elasticity and viscosity ratio on the steady bifurcation picture

Unlike the critical Rayleigh number, Ra_c^s at the onset of stationary thermal convection, the amplitude of convection is strongly influenced by fluid elasticity and viscosity ratio. It is convenient to monitor the response of the Nusselt number, Nu , as Ra is increased in the post-critical range. The influence of fluid elasticity on the bifurcation picture is depicted in figure 8, where Nu is plotted against r for $E \in [0, 0.2]$, for $Rv = 3.75$ and $Pr = 7$. E is chosen relatively small to ensure that the exchange of stability between the conductive state and stationary roll pattern is valid. The figure indicates that fluid elasticity tends to prohibit heat transport, relative to a Newtonian fluid. The bifurcation is supercritical, reflecting a gradual increase in Nu as r slightly exceeds one. The inset shows the results obtained with the amplitude equation method. The comparison indicates good agreement between the two methods. However, the dynamical system approach requires much less computational effort compared to the solution of the amplitude equations. This effort can be considerable, especially in the presence of oscillatory instability (Martinez-Mardones *et al.* 1996). Figure 8 suggests that there is little influence of fluid elasticity or relaxation time on the amplitude of stationary convection when r is close to one. This observation is in agreement with the measurements of Liang & Acrivos (1972). It is important to observe that the physical significance of the branch curves in figure 8 becomes clear only when the stability of these branches is known. It is found that Prandtl number has less influence on the amplitude of stationary thermal convection. For fixed elasticity number and viscosity ratio, Nusselt number remains essentially the same as Pr varies from 1 to 1000.

The dependence of heat transport on elasticity is further illustrated in figure 9, where Nu is plotted against E for $r = 1.5$ and $Pr = 7$. To ensure the accuracy of the results, several truncation levels are examined, for $M \in [6, 14]$. Recall that for $M = 6$, the steady-state solution is the same as the Newtonian limit. The figure shows clearly

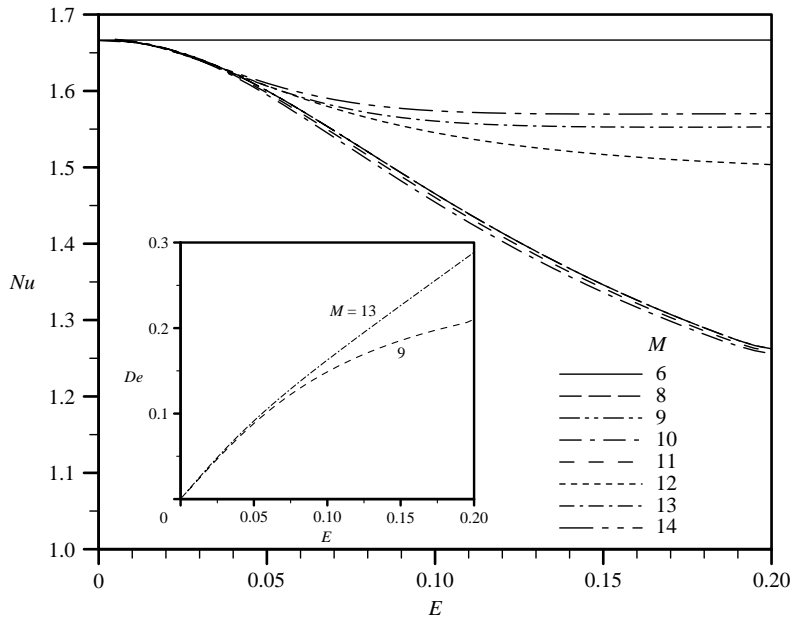


FIGURE 9. Influence of level of truncation on stationary thermal convection for $r = 1.5$, $Rv = 3.75$ and $Pr = 7$. The figure shows the dependence of the Nusselt number, Nu , on the elasticity number, E , for $M \in [6, 14]$. Note that the $M = 6$ curve corresponds also to a Newtonian fluid. The inset shows the dependence of De on E for $M = 9$ and 13 .

the influence of the nature and number of modes that must be included to ensure convergence (see also table 1). Regardless of the level of truncation for $M > 6$, the Nusselt number decreases with E . For small elasticity, the drop is sharp as suggested by figure 9, and is independent of the level of truncation. For a relatively small number of modes ($M = 8$ to 11), Nu continues to drop as E increases. This saturation or asymptotic behaviour occurs at smaller E as M increases. Figure 9 and table 1 clearly indicate that higher-order modes are needed ($M > 12$), once E exceeds 0.05 , for normal stress effects to be adequately represented.

So far, the elasticity number, E , has been taken as the only measure of normal stress effects in the results. E is defined as the ratio of the relaxation time and the diffusion time. This latter term, however, is not generally a suitable measure of the flow velocity time scale, and therefore may not adequately represent the influence of normal stresses (stemming from the upper-convective terms of the Oldroyd-B model). In contrast, the Deborah number, De , which is usually defined as the ratio of the characteristic relaxation time, λ , and a suitable hydrodynamic time scale, t^* , may be more representative of normal stress effect (Harder 1991). Almost all the literature on the thermal convection of viscoelastic fluids tends to neglect this issue; E is usually taken as the measure of elastic effects (Green 1968; Zielinska *et al.* 1986; Brand & Zielinska 1986; Rosenblat 1986; Larson 1992; Khayat 1995*a, b*; Kolodner 1998). Following Harder (1991), an *a posteriori* evaluation of De is conducted. The hydrodynamic time will be based on a velocity magnitude, V^* , averaged over the cell. For $M = 13$, the reference velocity magnitude $V^* = \sqrt{(\psi_{11} + \psi_{13})^2/k^2 + (\psi_{11} - \psi_{13}/3)^2/\pi^2}$. The inset in figure 9 shows the dependence of De on E for $M = 9$ and 13 . When a suitable number of normal stress modes are included ($M = 13$), De varies almost linearly with E for the range of E studied here, indicating that E is a suitable measure of elastic

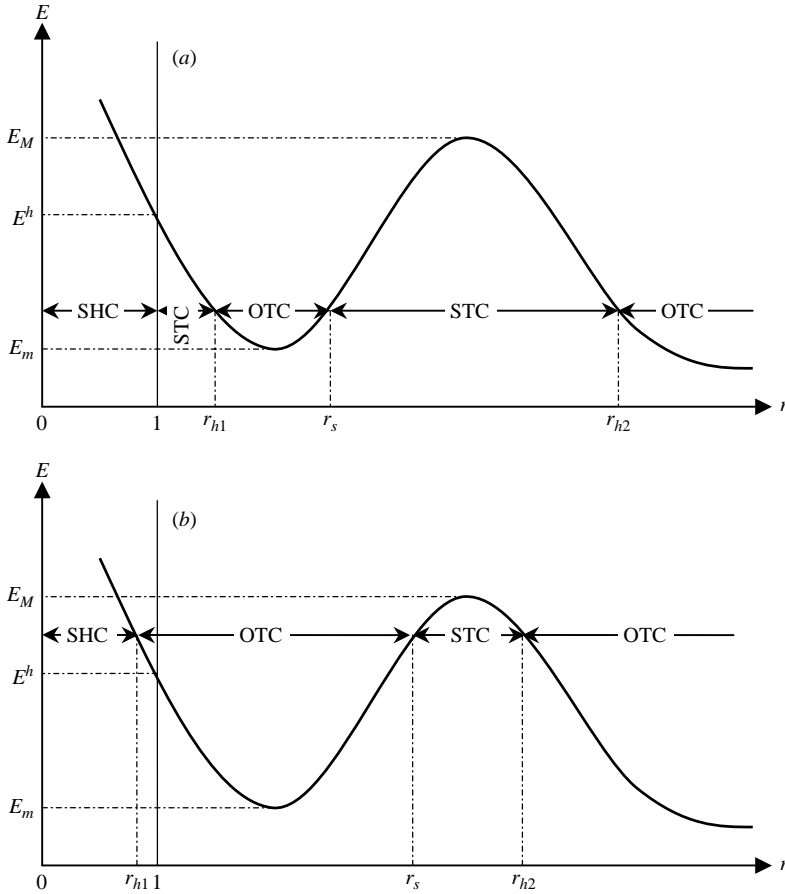


FIGURE 10. Schematic illustrating the critical regimes for (a) weakly ($E < E^h$) and (b) strongly ($E > E^h$) elastic fluids. The figure shows the ranges of stability for the various regimes: steady heat conduction (SHC), steady thermal convection (STC), and oscillatory thermal convection (OTC).

effects. In contrast, when normal stress effects are under-represented ($M = 9$), then De tends to be much smaller than E . Thus, normal stresses are overestimated when E is used. Note that for small E , both curves lead to an almost linear dependence of De on E .

4.3. Roll stability for weakly and strongly elastic fluids

In anticipation of the complex stability and bifurcation picture in the post-critical range, a preliminary summary of the qualitative picture is helpful at this stage. The overall stability picture and transition sequence for weakly and strongly elastic fluids are summarized in figure 10, which shows schematically the critical curve in the (E, r) -plane. It is recalled that weakly and strongly elastic fluids are defined as fluids with elasticity number $E < E^h(Rv, Pr)$ and $E > E^h(Rv, Pr)$, respectively. For a weakly elastic fluid, as the Rayleigh number increases from a small value, the steady heat conduction (SHC) loses its stability to stationary thermal convection (STC) at $r = 1$, similarly to a Newtonian fluid. Oscillatory thermal convection (OTC) emerges later at $r = r_{h1} > 1$, at which point a Hopf bifurcation emerges. There is a narrow range ($1 < r < r_{h1}$) for which STC is stable. The OTC is lost to STC at $r = r_s > r_{h1}$.

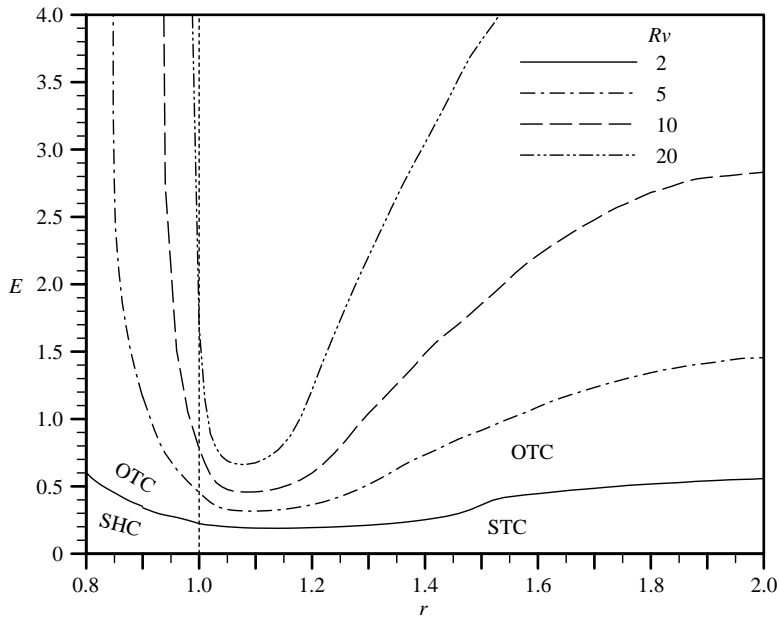


FIGURE 11. Influence of viscosity ratio on the critical E curves for the loss of stability of stationary thermal convection for fluids with $Pr=7$. The stability regions of are indicated for the $Rv=2$ curve. SHC, STC and OTC represent steady heat conduction, stationary heat convection and oscillatory heat convection states, respectively.

Finally, calculations show that OTC is regained at some $r=r_{h2} > r_s$. However, three-dimensional calculations seem to suggest that r_{h2} is generally beyond the range of validity of two-dimensional theory. Note that for a Newtonian fluid, there is only one transition, namely from STC to OTC. For a strongly elastic fluid, OTC emerges at $r=r_{h1} < 1$, and remains stable even when r exceeds 1. Note that r_{h1} is equal to r_c^h in this case. STC sets in at $r=r_s > 1$, which is lost at $r=r_{h2} > r_s$. In fact, stationary thermal convection is not likely to be observed (at least near $r=1$) for highly elastic fluids since oscillatory behaviour sets in at $r < 1$ as is established from linear stability analysis.

These observations are quantitatively substantiated in figure 11, which shows the critical curves in the (E, r) -plane for $Rv \in [2, 20]$ and $Pr=7$. The range $Rv \geq 2$ is deliberately chosen since for smaller Rv two-dimensional rolls are not expected to be observed (see below). The various stable regimes are explicitly shown for $Rv=2$. In the pre-critical range ($r < 1$), the SHC is stable for a point below the Rv curve. In the post-critical range ($r > 1$), STC is stable (unstable) for a point below (above) the Rv curve. The figure indicates that the region of stability of STC widens as the viscosity ratio increases. In this regard, it is noted that as $Rv \rightarrow \infty$, stationary convection is stable for the whole range of r values covered in the figure. In contrast, for a polymeric solution with small viscosity ratio, steady rolls appear to be stable only over a small range of elasticity number; in this case the region of stability appears to be uniform with r ($E < 0.3$ for $Rv=2$). More importantly, Rv has little influence on steady roll stability at small Rayleigh number ($r < 1.2$). In the range $r > 2$, each Rv curve exhibits a maximum, $E = E_M$, which is evident for the $Rv=10$ curve. The overall influence of the Prandtl number on the stability of steady rolls is similar to that of the viscosity ratio, Rv , which is shown in figure 11. The roll stability is essentially unaffected by

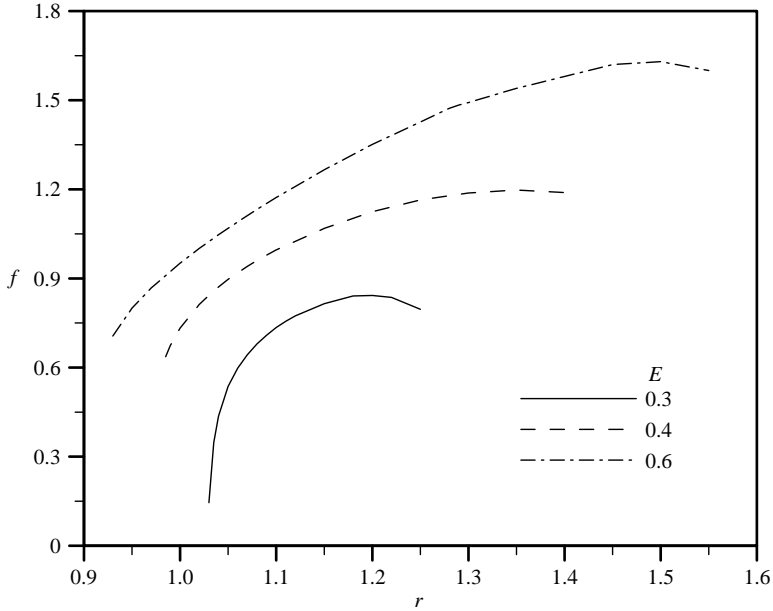


FIGURE 12. The influence of fluid elasticity for $E \in [0.3, 0.6]$ on the dominant frequency of oscillation for a fluid with $Rv = 3.75$ and $Pr = 7$.

Pr for $r < 1.5$. Generally, however, steady convection appears to be favoured for the more viscous polymeric solutions (large Pr).

It is finally helpful to examine the frequency of OTC. As observed earlier, stability analysis of the steady rolls suggests that STC loses its stability to oscillatory convection for the first time as the reduced Rayleigh number reaches $r = r_{h1}$. This is typically the case for fluids of small to moderate elasticity. Once r increases beyond r_{h1} , finite-amplitude oscillation emerges over the range $[r_{h1}, r_s]$. Figure 12 shows the influence of fluid elasticity for $E \in [0.3, 0.6]$ on the dominant frequency of oscillation, for $Rv = 3.75$ and $Pr = 7$. The figure indicates that, for a fluid with a given level of elasticity, the dominant frequency increases with r , but can display a maximum for relatively small elasticity. There is a jump (from zero) in the frequency at $r = r_{h1}$, which becomes sharper as E increases. The range $[r_{h1}, r_s]$ is clearly evident for each E curve, which widens as E increases. Thus, the range is $[1.03, 1.25]$, $[0.98, 1.4]$ and $[0.93, 1.57]$ for $E = 0.3, 0.4$ and 0.6 . It is interesting to observe that oscillatory thermal convection sets in at a higher frequency for the more elastic fluids. Figure 12 suggests an increase of f that is less than linear with E .

4.4. Roll, hexagonal and square patterns

After having examined the stability and bifurcation for the roll pattern, an important question remains as to whether the two-dimensional convective roll is the preferred pattern; in other words, what is the validity range for the two-dimensional formulation? Parmentier *et al.* (2000) carried out a weakly nonlinear stability analysis of Bénard–Marangoni convection of viscoelastic fluids using an amplitude-equation method. Three cell patterns consisting of rolls, hexagons, and squares were examined for stationary thermal convection; overstability was not considered. They also examined Rayleigh–Bénard convection (without surface tension). The upper surface was assumed to be adiabatically insulated. The roll pattern was predicted to be stable

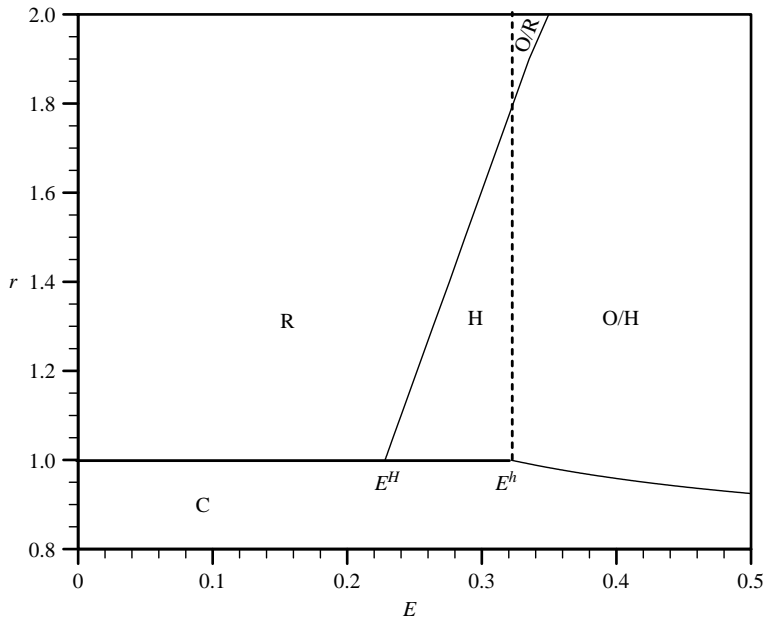


FIGURE 13. Stability picture obtained with amplitude equation method for two convection patterns, namely rolls and hexagons. This figure shows the stable range of roll and hexagonal patterns on the (r, E) -plane for a fluid with $Pr = 1000$ and $Rv = 3.75$. H and R represent stable regions for hexagonal and roll patterns, respectively, C the stable heat conduction state, and O the oscillatory convection. E^H represents the critical elasticity number for the emergence of three-dimensional convective pattern (hexagon), while E^h has the same meaning as before.

only for small elasticity number ($E < 0.0035$) near criticality. The three-dimensional hexagonal pattern was found to be stable for $E \in [0.0035, 0.07]$, for a fluid with $Pr = 1000$ and $Rv \approx 0.01$. The square pattern was found to be always unstable (at least near criticality). It is observed that, according to the current linear stability analysis, the limit $E = 0.07$ corresponds to the critical elasticity number for the emergence of overstability. In this section, a similar amplitude equation method is used to examine parameter ranges of three-dimensional stationary convection that have not been covered by Parmentier *et al.* (2000), and, simultaneously, to establish the range of validity of the roll pattern. The stability of the steady rolls, hexagons and squares is determined through linear stability analysis of the steady-state solutions of equations (30) to (36) pertaining to each pattern.

The current calculations are based on the free–free boundary conditions only, and indicate that the viscosity ratio has a strong influence on the stable ranges of stationary roll and hexagonal patterns. The square pattern is also found to be always unstable. The stability picture is best illustrated in the (r, E) -plane. Figure 13 shows typical regions of existence of roll and hexagonal patterns for a fluid with $Rv = 3.75$ and $Pr = 1000$. In the figure, H and R indicate stable hexagonal and roll regions, respectively. In contrast to the prediction of Parmentier *et al.* (2000), there is no region where both hexagon and roll patterns coexist, as a result of the use of different boundary conditions here. Despite this discrepancy, qualitative agreement is obtained regarding the stable ranges of hexagonal and roll patterns. For relatively small E , the conductive state, C , is lost to two-dimensional stationary convection (rolls) when r exceeds unity. When the level of elasticity exceeds a critical value E^H ,

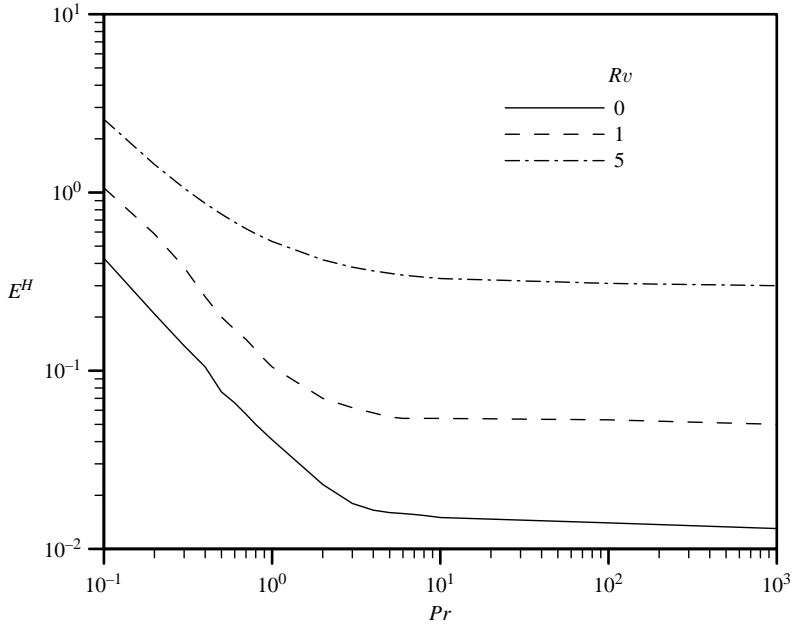


FIGURE 14. Influence of Pr on the critical elasticity number E^H for different value of Rv . The curves show that E^H decreases monotonically with Pr .

but remains smaller than E^h , only the hexagonal pattern is stable at the onset of stationary convection. Beyond E^h , oscillatory convection sets in. It is found that E^H increases linearly with r , which seems to be the case for other values of Rv and Pr . Thus, rolls are expected to be more stable at higher Rayleigh number. The figure also indicates that E^H can be larger than E^h at higher Rayleigh number, which means that both stationary roll and oscillatory convection become possible. This region is indicated by O/R in the figure. For $E > E^h$, the conductive state loses its stability at $r < 1$ as predicted by linear stability analysis. Similarly, there is a region marked by O/H, where both stationary hexagons and oscillatory convection are possible.

The dependence of E^H on the fluid parameters is summarized in figures 14 and 15, where E^H is plotted against Pr and Rv at $r = 1.1$, respectively. Figure 14 shows the influence of Pr on E^H for $Rv \in [0, 5]$. It is interesting to observe that the dependence of E^H on Pr is similar to that of E^h (see figure 2). Two distinct regimes can be discerned from figure 14. For small Pr values, E^H drops sharply like $Pr^{-0.93}$ regardless of the viscosity ratio. In this range, the roll pattern appears to be preferred unless E is relatively large. Thus, rarefied gases ($Pr \ll 1$ and $Rv = 0$) would exhibit a predominantly roll pattern! For larger Pr values, E^H remains essentially constant. The curves become flattened, which indicates that for typical polymeric solutions ($Pr \gg 1$), the influence of Pr on the stationary convective patterns is not significant. Thus, it is the viscosity ratio of the polymeric solution that determines the likelihood for two- or three-dimensional convection. Note that E^H tends to infinity, for any Pr , in the limit of a Newtonian fluid ($Rv \rightarrow \infty$). This can be seen more clearly from figure 15, which shows the increase of E^H with Rv for several values of Pr . The increase is slow when Rv is relatively small. For large Rv , the figure indicates that E^H is simply proportion to Rv , and this behaviour may be given by

$$E^H \approx 0.07Rv - 0.022 \quad (Pr \gg 1) \quad (41)$$

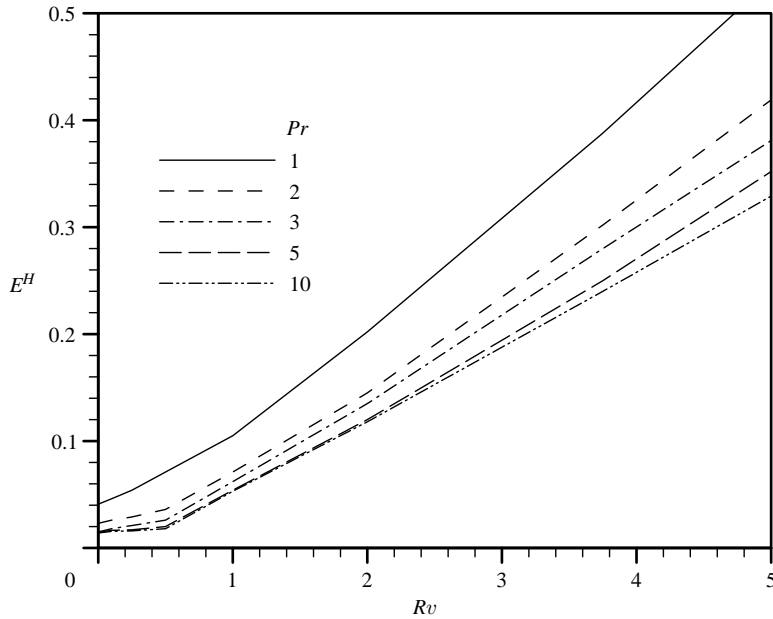


FIGURE 15. Influence of Rv on the critical elasticity number E^H for different value of Pr . The curves show the linear dependence of E^H on Rv when $Rv > 0.5$.

Thus, in contrast to elasticity, viscosity ratio tends to prohibit three-dimensional and oscillatory convection. The stable range of two-dimensional roll pattern is significantly widened with increasing Rv , which is of course expected as the contribution of the Newtonian solvent increases. Recall, that in the Newtonian limit, only rolls are predicted, regardless of the nature of boundary conditions used (Schlüter, Lortz & Busse 1965).

5. Conclusion

The finite-amplitude thermal convection for a thin layer of a viscoelastic fluid of the Oldroyd-B type is examined in this study. The conditions for the onset of stationary and oscillatory rolls, and their subsequent form in the post-critical range, are emphasized. A nonlinear dynamical system is derived by spectrally expanding the flow field and applying the Galerkin projection method. Two main regimes are identified, which correspond to weakly elastic and strongly elastic fluids. A weakly (strongly) elastic fluid is identified as a fluid with elasticity number $E < E^h$ ($E > E^h$), where E^h is the critical elasticity number for the onset of oscillatory convection (Hopf bifurcation). In this case, the transition to oscillatory convection occurs in the post-critical (pre-critical) range of the Rayleigh number, corresponding to $r < 1$ ($r > 1$). For a weakly elastic fluid, steady heat conduction is unconditionally stable in the pre-critical range, $r < 1$. At $r = 1$, steady heat conduction is lost to stationary thermal convection similarly to a Newtonian fluid, which remains stable over a relatively small range of Rayleigh numbers. Oscillatory thermal convection emerges if the Rayleigh number is further increased. For a strongly elastic fluid, steady heat conduction is lost directly to oscillatory thermal convection in the pre-critical range, $r < 1$. In contrast to weakly elastic fluids, oscillatory thermal convection remains stable even when r exceeds 1. Stationary thermal convection emerges when the Rayleigh number increases

further (refer to figure 10). The effect of elasticity on oscillatory thermal convection in the pre-critical range, $r < 1$, is examined in some detail, and the sequence of flow behaviour is reported in figures 6 and 7. This behaviour is reminiscent of the flow sequence observed by Muller *et al.* (1993) for Taylor–Couette flow as E is increased beyond the critical threshold. In the present problem, the route to chaos is clearly identified as corresponding to the Curry–Yorke model or the breakup of a T^2 torus.

A weakly nonlinear approach is used to study the stability of stationary convective patterns, namely rolls, hexagons and squares, in the post-critical range of the Rayleigh number. Six Landau-type amplitude equations are derived by following a generalized method proposed by Parmentier *et al.* (2000). Stationary hexagonal patterns are predicted to be stable for a certain range of elasticity number, which is in contrast to the Newtonian case, where only rolls are predicted to be stable. The influence of the Prandtl number and the viscosity ratio on the stability of rolls and hexagons is examined. It is found that the viscosity ratio plays a more important role in determining the likelihood of the two- or three-dimensional patterns for typical polymeric solutions.

The financial support of the Natural Sciences and Engineering Research Council is gratefully acknowledged.

REFERENCES

- BIRD, R. B., ARMSTRONG, R. C. & HASSAGER, O. 1987 *Dynamics of Polymeric Liquids*, vol. 1, 2nd edn. John Wiley & Sons.
- BOGER, D. V & WALTERS, K. 1993 *Rheological Phenomena in Focus*. Elsevier.
- BRAND, H. R. & ZIELINSKA B. J. 1986 Tri-critical codimension-2 point near the onset of convection in viscoelastic liquids. *Phys. Rev. Lett.* **57**, 3167.
- CROSS, M. C. & HOHENBERG, P. C. 1993 Pattern formation outside of equilibrium. *Rev. Mod. Phys.* **65**, 851.
- CURRY, J. & YORKE, J. A. 1977 A transition from Hopf bifurcation to chaos: computer experiments with maps in R^2 , In *The Structure of Attractors in Dynamical Systems*. Springer Notes in Mathematics, vol. 668, p. 48. Springer.
- DRAZIN, P. G. & REID, W. H. 1981 *Hydrodynamic Stability*. Cambridge University Press.
- ECKHAUS, W. 1965 *Studies in Non-linear Stability Theory*. Springer.
- ELTAYEB, I. A. 1977 Nonlinear thermal convection in an elasticoviscous layer heated from below. *Proc. R. Soc. Lond. A* **356**, 161.
- FRIEDMAN, B. 1956 *Principles and Techniques of Applied Mathematics*. John Wiley & Sons.
- GREEN, T. 1968 Oscillating convection in an elasticoviscous liquid. *Phys. Fluids* **11**, 1410.
- HARDER, H. 1991 Numerical simulation of thermal convection with Maxwellian viscoelasticity. *J. Non-Newtonian Fluid Mech.* **36**, 67.
- KELLY, R. E. & PAL, D. 1978 Thermal convection with spatially periodic boundary conditions: resonant wavelength excitation. *J. Fluid Mech.* **86**, 433.
- KHAYAT, R. E. 1994 Chaos and overstability in the thermal convection of viscoelastic fluids. *J. Non-Newtonian Fluid Mech.* **53**, 227.
- KHAYAT, R. E. 1995a Nonlinear overstability in the thermal convection of viscoelastic fluids. *J. Non-Newtonian Fluid Mech.* **58**, 331.
- KHAYAT, R. E. 1995b Fluid elasticity and the onset of chaos in thermal convection. *Phys. Rev. E* **51**, 380.
- KHAYAT, R. E. 1995c Onset of Taylor vortices and chaos in viscoelastic fluids. *Phys. Fluids* **7**, 2191.
- KHAYAT, R. E. 1996 Onset of chaos in the thermal convection of weakly shear thinning fluids. *J. Non-Newtonian Fluid Mech.* **63**, 153.
- KHAYAT, R. E. 1997 Low-dimensional approach to nonlinear overstability of purely elastic Taylor-vortex flow. *Phys. Rev. Lett.* **78**, 4918.

- KHAYAT, R. E. 1999 Finite-amplitude Taylor-vortex flow of viscoelastic fluids. *J. Fluid Mech.* **400**, 33.
- KHAYAT, R. E. & EU, B. C. 1989 Generalized hydrodynamics, normal stress effects and velocity slip in the cylindrical Couette flow of Lennard-Jones fluids. *Phys. Rev. A* **39**, 728.
- KOLODNER, P. 1998 Oscillatory convection in viscoelastic DNA suspensions. *J. Non-Newtonian Fluid Mech.* **75**, 167.
- LARSON, R. G. 1988 *Constitutive Equations for Polymer Melts and Solutions*. Butterworths.
- LARSON, R. G. 1992 Instabilities in viscoelastic flows. *Rheol. Acta* **31**, 213.
- LI, Z. 2003 Study on thermal convection and rotating flow for Newtonian and non-Newtonian fluids. PhD thesis, the University of Western Ontario, London, Ontario, Canada.
- LIANG, S. F. & ACRIVOS, A. 1970 Experiments on buoyancy driven convection in non-Newtonian fluids. *Rheol. Acta* **9**, 447.
- LORENZ, E. N. 1963 Deterministic nonperiodic flows. *J. Atmos. Sci.* **20**, 130.
- MARTÍNEZ-MARDONES, J. & PÉREZ-GARCÍA, C. 1990 Linear instability in viscoelastic fluid convection. *J. Phys.: Condens. Matter* **2**, 1281.
- MARTÍNEZ-MARDONES, J. & PÉREZ-GARCÍA, C. 1992 Bifurcation analysis and amplitude equations for viscoelastic convective fluids. *Il Nuovo Cimento* **14**, 961.
- MARTÍNEZ-MARDONES, J., TIENMANN, R., WALGRAEF, D. & ZELLER, W. 1996 Amplitude equations and pattern selection in viscoelastic convection. *Phys. Rev. E* **54**, 1478.
- MCLAUGHLIN, J. B. & MARTIN, P. C. 1975 Transition to turbulence in a statically stressed fluid system. *Phys. Rev. A* **12**, 186.
- MULLER, S. J., SHAQFEH, E. S. G. & LARSON, R. G. 1993 Experimental study of the onset of oscillatory instability in viscoelastic Taylor-Couette flow. *J. Non-Newtonian Fluid Mech.* **46**, 315.
- NEWELL, A. C., PASSOT, T. & LEGA, J. 1993 Order parameter equations for patterns. *Annu. Rev. Fluid Mech.* **25**, 399.
- NEWHOUSE, S., RUELLE, D. & TAKENS, T. 1978 Occurrence of strange Axiom-A attractors near quasi-periodic flows near T^m $m \geq 3$. *Commun. Math. Phys.* **64**, 35.
- PARK, H. M. & LEE, H. S. 1996 Hopf bifurcations of viscoelastic fluids heated from below. *J. Non-Newtonian Fluid Mech.* **66**, 1.
- PARMENTIER, P., LEBON, G. & REGNIER, V. 2000 Weakly nonlinear analysis of Bénard-Marangoni instability in viscoelastic fluids. *J. Non-Newtonian Fluid Mech.* **89**, 63.
- ROSENBLAT, S. 1986 Thermal convection of a viscoelastic fluid. *J. Non-Newtonian Fluid Mech.* **21**, 201.
- SCHLÜTER, A., LORTZ, D. & BUSSE, F. 1965 On the stability of steady finite amplitude convection. *J. Fluid Mech.* **23**, 130.
- SOKOLOV, M. & TANNER, R. I. 1972 Convective stability of a general viscoelastic fluid heated from below. *Phys. Fluids* **15**, 534.
- TANNER, R. I. 1983 *Engineering Rheology*. Oxford University Press.
- VEST, C. M. & ARPACI, V. S. 1969 Overstability of a viscoelastic fluid layer heated from below. *J. Fluid Mech.* **36**, 613.
- WALTERS, K. 1980 *Rheometry: Industrial Applications*. Research Studies Press.
- ZIELINSKA B. J., MUKAMEL, D. & STEINBERG, V. 1986 Multicriticality in viscoelastic fluids heated from below. *Phys. Rev. E* **33**, 1454.